

RESEARCH

Open Access



Effect of cisplatin/gold chitosan nanocomposite on oral squamous cell carcinoma and oral epithelial cells

Basma Abdelrahman Ahmed^{1*}, Rania Osama M. Mohsen², Marwa Sharaky³, Marwa A. Ramadan⁴, Amna H. Faid⁵ and Mai Hafez Mohamed⁶

*Correspondence:
basmaabdelrahman@dent.asu.edu.eg

¹ Oral Pathology Department, Faculty of Dentistry, Ain Shams University, Cairo, Egypt

² Oral Biology Department, Faculty of Dentistry, Ain Shams University, Cairo, Egypt

³ Pharmacology Unit, Cancer Biology Department, National Cancer Institute, Cairo University, Giza, Egypt

⁴ Department of Laser Application in Metrology, Photochemistry and Agriculture, National Institute of Laser Enhanced Science (NILES), Cairo University, Giza, Egypt

⁵ Department of Laser Sciences and Interactions, National Institute of Laser Enhanced Science (NILES), Cairo University, Giza 12613, Egypt

⁶ Oral Pathology Department, Faculty of Dentistry, British University in Egypt, Cairo, Egypt

Abstract

Background: Oral squamous cell carcinoma (OSCC) treatment represents a great challenge, since platinum-based therapeutic agents have deleterious effects on normal cells and tissues. Employing gold nanoparticles (AuNps) as carriers for cisplatin have proved effective in reducing cisplatin doses. Green synthesis of AuNps from eco-friendly agents like chitosan improves the AuNps' biocompatibility and cytotoxicity. Thus, we synthesized a novel agent of cisplatin coupled to gold chitosan nanoparticles (Cis/AuCh nanocomposite) and examined its effect in addition to the effect of chitosan-reduced gold nanoparticles (AuCh Nps) on (HNO97) OSCC cell line and normal oral epithelial cells (OEC).

Results: Ultraviolet–visible spectroscopic analysis, transmission electron microscope, X-ray diffraction, and Fourier transform infrared spectroscopy confirmed the successful synthesis of AuCh Nps and Cis/AuCh nanocomposite. The cytotoxicity assay showed that the IC50 doses of AuCh Nps and Cis/AuCh nanocomposite after 48 h were 12.5 µg/ml, and 6.2 µg/ml, respectively, on the HNO97 cell line. On the other hand, the IC50 doses were 40 µg/ml and 44.5 µg/ml on OEC, respectively. After treating both cell lines with the HNO97–IC50 doses, Cis/AuCh nanocomposite-treated HNO97 cell line revealed a significant rise in Caspase 3 immunohistochemical apoptotic index, besides a significant elevation in pro-apoptotic proteins and reduction in Bcl-2 compared to cisplatin. Conversely, opposite results were detected in AuCh Nps and Cis/AuCh nanocomposite-treated OEC. Flow cytometry results revealed S and G2/M shifts in HNO97 and OEC with more shift in the cisplatin-treated group than AuCh Nps and Cis/AuCh nanocomposite-treated groups in both cell lines. The expressions of the reactive oxygen species (ROS) markers; malondialdehyde and nitric oxide were the highest in Cis/AuCh nanocomposite-treated HNO97, while the reduced glutathione expression was the lowest. However, AuCh Nps and Cis/AuCh nanocomposite-treated groups did not display any significant changes in ROS markers expression from the untreated group in the OEC.

Conclusions: AuCh NPs can be considered a good alternative way of cisplatin transportation for OSCC treatment. Cis/AuCh nanocomposite stimulates apoptosis,



cell cycle arrest, and ROS production in oral cancer cells with less undesired effects on normal oral epithelial cells.

Keywords: Oral squamous cell carcinoma, Oral epithelial cells, Cisplatin, Gold nanoparticles, Chitosan, Apoptosis, Cell cycle, Reactive oxygen species

Background

Oral cavity cancer is one of the most frequent head and neck malignancies, ranking 16th globally, where more than 90% of them are oral squamous cell carcinoma (OSCC). OSCC represents the most aggressive epithelial malignant neoplasm (Chamoli et al. 2021). Patients are treated with different therapies depending on the type and stage of cancer, either traditional treatment, such as surgery, radiation, and chemotherapy or novel therapies like immunotherapy (Zhang and Chen 2018), targeted therapy (Troy and Baudino 2015), gene therapy (Das et al. 2015), and photothermal therapy (Faid et al. 2022; Ramadan and El-Tayeb 2023).

Cis-diamminedichloroplatinum II (Cisplatin) is one of the platinum-based chemotherapeutic drugs, used for solid cancer treatment (Ho et al. 2016). Cisplatin binds and damages DNA, thus, blocks the production of mRNA, and multiple proteins, and activates several pathways that induce necrosis or apoptosis (Dasari and Tchounwou 2014). Meanwhile, cisplatin shows several drawbacks because of the drug's related cancer relapse, adverse effects, and resistance (Rocha et al. 2018; Skowron et al. 2018). In addition, many toxicities arise from cisplatin treatment (Dasari and Tchounwou 2014; Oun et al. 2018). To minimize the adverse effects and resistance of cisplatin, combination therapies are adopted and have proven to be more effective in cancer therapy (Ghosh 2019; Faid and Ramadan. 2024).

Nanotechnology has acquired a substantial interest, where nanoparticles have been recognized for their potential usefulness in biomedical applications (Gulati et al. 2021; Hashem et al. 2022; Faid et al. 2024; Ramadan et al. 2024a). The nanotechnological approaches were employed to improve the bioavailability of large molecular weight agents (Javed et al. 2020), increase the permeability to biological barriers, and improve drug transportation (Cheng et al. 2021a).

Loading chemotherapeutic drugs on nanoparticles is a confirmed effective method to protect cancer patients from drug toxicity (Cheng et al. 2021a). Polymeric nanoparticles, nanoemulsions, lipid-based nanoparticles, carbon-based nanoparticles, quantum dots, monoclonal antibodies, extracellular vesicles, and metallic nanoparticles are the most commonly manufactured nanoparticles for drug delivery (Almessori et al. 2021; Ansari et al. 2021; Cheng et al. 2021a; Jafari-Gharabaghloou et al. 2023).

Various studies were conducted to confirm the efficacy of loading nanoparticles with anticancer cytotoxic agents in different cell lines (Khan et al. 2020; Pourgholi et al. 2021; Alagheband et al. 2022). The studies usually focus on the effect of these nanoparticles on the critical pathways of carcinogenesis controlling cell death, proliferation, cell cycle, and reactive oxygen species (ROS) production (Khan et al. 2018; Pourgholi et al. 2021; Hasani et al. 2022; Jafari-Gharabaghloou et al. 2023; Zhang et al. 2023) or specific mutated genes that affect carcinogenesis in different cancer types (Alagheband et al. 2022; Kho-shravan Azar et al. 2022).

Gold nanoparticles (AuNps) are one of the most generally utilized nanoparticles in biomedical applications because of their unique characteristics of size, shape, optical properties, biocompatibility, and low cytotoxicity (Bansal et al. 2020; Nejati et al. 2022; Hamdy et al. 2024). In addition, their efficacious target specificity, and enhanced rate of cellular uptake render them an excellent option for cell death induction in various cancer cell lines (González-Ballesteros et al. 2017; Martínez-Torres et al. 2018).

They can be synthesized by biological methods, using microorganisms, enzymes, and/or biodegradable polymers derived from plants or animals. These biological methods have been proposed to be environmentally friendly approaches. They substitute the chemical and physical ways, providing an opportunity to be used in biomedical fields safely (Mohanpuria et al. 2008; Bagci et al. 2015). The effect of nanoparticles on cancerous and healthy cells is determined by the reducing agent. Chitosan is obtained from chitin polymer deacetylation that is present naturally in the prawns and crustaceans shells (Li et al. 2022).

There are several applications for chitosan. Drug delivery has taken advantage of chitosan's positive charge, which permits non-covalent interactions with biological tissues and might help to overcome the shortcomings of current chemotherapy. Furthermore, chitosan has the potential to accumulate at the tumor site, trigger M1 macrophage polarization, and change the tumor microenvironment from immunosuppressive to immunosupportive, all of which might have an anticancer impact and increase the effectiveness of cancer immunotherapy. Finally, but just as potentially, chitosan itself may prevent the proliferation of tumor cells, angiogenesis generated by tumors, and tumor metastasis. As a result, chitosan and its derivatives may work very well in the domain of cancer treatment (Ding and Guo 2022).

Using chitosan as a reducing and capping agent with AuNps, forming chitosan-reduced gold nanoparticles (AuCh Nps), can decrease their aggregation, stabilizing them as well as raise their biocompatibility, biodegradability, and cytotoxicity to cancerous cells (Collado-González et al. 2015; Gulati et al. 2021; Ramadan et al. 2024b).

Gold nanoparticles became one of the promising drug delivery vehicles for platinum chemotherapeutic agents (Chen et al. 2017). Using AuNps for transporting cisplatin, reduces its dose with the same effect as the free drug, thus decreasing its undesired adverse effects (González-López et al. 2020). Furthermore, the preferences of applying AuNps as a drug nanocarrier are the release of drugs in a consistent regulatory way, drug targeting selectivity, enhanced cellular uptake of platinum-based agents, ability to sensitize the cells to chemotherapeutic drugs, and resistance to degradation by enzymes (Ma et al. 2015; Wróblewska et al. 2022).

Although past research has fundamentally focused on the synthesis of AuCh Nps demonstrating their anticancer properties and biocompatibility, the role of these nanoparticles as chemotherapeutic carriers and their anticancer effect on various malignancies have not been fully addressed in the literature. Thus, in this study, cisplatin was loaded on AuCh Nps, forming a newly synthesized Cis/AuCh nanocomposite in an attempt to investigate the anticancer effect and mechanism of action of this nanocomposite for the first time on OSCC cell line and detect its possible safety on normal oral epithelial cells (OEC).

Consequently, the present study aimed to examine the antitumor effect of AuCh Nps and Cis/AuCh nanocomposite, regarding cytotoxicity, apoptosis, cell cycle regulation, and ROS status on OSCC and OEC cell lines, in addition to comparing their effects to that of cisplatin.

Materials and methods

Chemicals and reagents

Cisplatin was obtained from MYLAN Company, France. Acetic acid and the aqueous solution of HAuCl_4 were obtained from Sigma Aldrich Chemical Co., St. Louis, Mo, USA. Dulbecco's Modified Eagle Medium (DMEM) medium, Penicillin Streptomycin (Pen Strep), and Trypsin were purchased from Gibco Life Technologies, USA. Heat-inactivated fetal bovine serum (HFBS) was obtained from Invitrogen Co., Waltham, MA, USA. Sulforhodamine B (SRB) (Catalog No. ab235935) and the primary antibody Anti-Caspase 3, rabbit recombinant monoclonal antibody for immunohistochemical (IHC) staining (Catalog No. ab184787) were supplied from abcam, Cambridge, UK. Biotinylated goat anti-rabbit antibody and streptavidin-peroxidase were purchased from Thermo Fisher Scientific, Waltham, Massachusetts, USA, and Horseradish peroxidase (HRP) ADVANCETM/HRP was obtained from Dako, Carpinteria, CA, USA. Diaminobenzidine Tetrahydrochloride (DAB) chromogen was supplied from Sigma, St. Louis, MO, USA. Enzyme-linked immunosorbent assay (ELISA) kits for Caspase 3 (Catalog No. SEA626Hu), Bax (Catalog No. SEB343Mu), Bcl-2 (Catalog No. SEA778Ra), P53 (Catalog No. SEH009Hu), and Caspase 8 (Catalog No. MBS452285) were attained from cloud Clone Corp, (USA). Malondialdehyde (MDA) Assay Kit (Catalog No. MAK085), and Ellman's reagent [5,5-dithiobis-(2-nitrobenzoic acid)] for Glutathione (GSH) measurement were purchased from Sigma Aldrich St. Louis, MO, USA.

Preparation of AuCh Nps and Cis/AuCh nanocomposite

For AuCh Nps preparation, 1 gm of medium molecular weight chitosan was dissolved in 100 ml of 1% acetic acid boiled on a hot plate. Then 10 μL of 1.25×10^{-1} M concentrated aqueous solution of HAuCl_4 was added to 10 ml of chitosan solution. Next, the mixture was heated for 15 min at 100 °C while stirring constantly to create a red color (Faid et al. 2023). Subsequently, Cis/AuCh nanocomposite was formed by coating AuCh Nps with cisplatin. 1 ml of cisplatin (1 mg/ml) was mixed with 1 ml of the synthesized AuNps dropwise and sonicated for 20 min.

Characterization of AuCh Nps and Cis/AuCh nanocomposite

Ultraviolet–visible (UV–Vis) spectroscopic analysis

A double beam spectrophotometer (PG instrument, T80⁺, UK) was used to detect the absorption spectra of the formed samples. 2 ml of the prepared solutions were obtained by diluting 200 μl of the solution with distilled water, followed by a transfer to a 1 cm UV-quartz cell. The absorption spectra were recorded within the proper scan range (200 nm to 800 nm).

Transmission electron microscope (TEM) measurements

The morphology of the prepared solutions was obtained using TEM at the Nanotechnology and Advanced Material Central Lab. (NAMCL), Agriculture Research Center (ARC), Giza, Egypt. Company name: FEI, Netherlands. Model: Tecnai G20, Super twin, double tilt and Applied voltage: 200 kV, Magnification Range: up to 1,000,000 X and Gun type: LaB6 Gun. A monolayer was produced by adding drops of a very dilute solution on an amorphous carbon-coated copper grid which was left to evaporate at room temperature, then imaged by TEM.

Dynamic light scattering (DLS) analysis and zeta potential

The particle size and surface charges of Auch Nps and Cis/AuCh nanocomposite were inspected by DLS with Zeta sizer 300 HAS (Malvern Instruments, Malvern, UK) depending on photon correlation spectroscopy. After 60s of analysis, the average zeta potential was determined. Nanoparticulate dispersion zeta potential was obtained without dilution.

Fourier transform infrared spectroscopy (FT-IR) analysis

Measurements of the FT-IR were conducted using a (4100 Jasco-Japan, FT-IR spectrometer). The samples of Auch Nps and Cis/AuCh nanocomposite were freeze-dried by a lyophilizer, powdered, and diluted with potassium bromide (KBr). Then the IR spectra were measured in the range of 500–4500 cm^{-1} .

X-ray diffraction (XRD) analysis

Phase analysis was detected with the XRD technique (X'pert PRO, PAN analytical, Almelo, the Netherlands) in the scanning mode conducted at 40 kV and a current of 30 mA with Cu K radiation ($= 1.54 \text{ \AA}$) and High Score Plus software. The standard International Center for Diffraction Data (ICDD) library was the reference for comparing the diffraction intensities. The source of data about the synthesized nanomaterial crystal structure was the Powder Diffraction File (PDF-4) database.

Cell culture and cell lines

Tongue squamous cell carcinoma (HNO97) and OEC cell lines were obtained from the National Cancer Institute, Cairo University, (Giza, Egypt). The cell lines were maintained in a DMEM medium containing 10% HFBS and 1% Pen Strep. The cell lines were kept in a 5% CO_2 incubator at 37 °C and a humidified atmosphere. After reaching 80% cell confluency, trypsinization was done and cells were subcultured.

Sulphorhodamine-B (SRB) and IC50 calculation

The cytotoxic effect of cisplatin, AuCh Nps, and Cis/AuCh nanocomposite was detected by SRB assay (Vichai and Kirtikara 2006; Sharaky et al. 2020). The 5n passage of cells was used for this test. Briefly, the cells were seeded in a 96-well cell culture plate (cells density 3×10^3 cells/well) in a 100 μl complete growth medium and maintained in the incubator at 37 °C for 24 h. Each test included a blank well containing a complete medium without cells and serial concentrations, of each drug, added individually. The plates were placed in the incubator for 48 h, then, examined by the inverted microscope and transferred to

a sterile work area for SRB assay. For each concentration, three wells were used. After 48 h, the cells were fixed with 20% trichloroacetic acid, and stained with 0.4% SRB dye. The optical density (O.D.) of each well was measured by a spectrophotometer at 570 nm using an ELISA microplate reader (TECAN sunrise™, Germany). The percentage of alive cells was calculated by the following equation:

$$\% \text{ Cell Viability} = \frac{(\text{O.D.}) \text{ mean of treated cells}}{(\text{O.D.}) \text{ mean of control untreated cells}} \times 100$$

Then the IC50 (concentration that produces 50% of cell growth inhibition) value for each drug on both cell lines was calculated using dose–response curve-fitting models (Graph Pad Prizm software, version 8).

The doses selected for the subsequent tests on both cell lines were the HNO97–IC50 doses for 48 h of cisplatin, AuCh Nps, and Cis/AuCh nanocomposite, in addition to untreated cells as negative control.

Detection of the cellular morphological changes

The cells were fixed in 50% ethanol and a cell pellet was obtained by centrifugation. After removal of the fixative, the cell pellet was dehydrated in 3 mL acetone. Melted paraffin was then applied on the dry warmed cell pellet and left to solidify and microscopic slides were obtained and stained with Hematoxylin and Eosin (H & E) (Krogerus and Anderson 1988; Bressenot et al. 2009). Six photos from each group were taken with the digital camera (Canon EOS 650D) mounted on the light microscope (BX60, Olympus, Japan) with magnification (1000X Oil immersion). The images were used for the determination of cellular and nuclear morphological changes.

Active Caspase 3 immunohistochemical (IHC) staining and determination of apoptotic index (AI)

Five μm thick sections from paraffin blocks of each group were deparaffinized. For heat-induced epitope retrieval, the sections were incubated at 120 °C for 10 min in 0.01 M sodium citrate solution (pH 6), followed by a 2 h cool down. The primary antibody anti-Caspase 3, rabbit recombinant monoclonal antibody with dilution 1:1000, was applied for 16 h at 4 °C. The sections were twice washed with phosphate-buffered saline with Tween 20 (PBS-T) (0.1MPBS, pH 7.4 and 0.1%Tween 20) over 10 min, then incubated at room temperature for an hour with biotinylated goat anti-rabbit antibody at dilution 1:200.

After two PBS-T washes (for 10 min each time), the activity of endogenous peroxidase was blocked by incubating the sections in a 6% hydrogen peroxide solution for 10 min. The slides were washed twice in PBS-T (5 min each), followed by incubation at room temperature for an hour in streptavidin-peroxidase at dilution 1:150. After two PBS-T washes, the sections were immersed in ADVANCETM/HRP and (DAB) chromogen for the visualization of antigen–antibody complexes. Finally, counterstaining was performed using half-diluted Harris hematoxylin (Bressenot et al. 2009).

Seven fields comprising at least 1000 cells from each group were captured with the digital camera (Canon EOS 650D) mounted on the microscope (BX60, Olympus, Japan) with magnification (1000X Oil immersion) and were used to detect the apoptotic index

(AI) of each group. AI represented the percentage of the counted caspase 3 labeled cells relative to the total number of cells in each field (Bressenot et al. 2009).

Determination of apoptotic markers by ELISA

The expressions of P53, Caspase 3, Caspase 8, Bax, and Bcl-2 in each cell line were evaluated with ELISA. HNO97 and OEC cell lines were applied to the plates at a density of 2×10^6 . Both cell lines were treated with the HNO97-IC50 doses. After incubation for 48 h, cells were collected by centrifugation at 1800g for 5 min, the culture media was discarded and the cells were twice washed with phosphate-buffered saline (PBS). Next the pellets were lysed in 50 μ l cold lysis buffer and the lysate was centrifugated at 12,000g for 1 min at 4 °C, and then the supernatant was collected (Reen 1994).

Bradford method was used to detect the protein levels of the markers (Kielkopf and Bauer 2020). According to the manufacturer's protocol; 100 μ l of the Detection Reagent A was added to each well containing 100 μ l of the standard or sample and incubated for 1 h at 37 °C. The solution was then aspirated and washed for 1–2 min with 350 μ l of 1 \times Wash Solution. 100 μ l of Detection Reagent B working solution was subsequently added to each well and the wells were incubated for 30 min at 37 °C, then the aspiration and wash were repeated. 90 μ l of the Substrate Solution was added to each well, and incubated for 20 min at 37 °C. 50 μ l of the Stop Solution was then added and the solution turned yellow. Finally, in a microplate reader (Biotech, Inc., USA), the color of each sample was recorded at 450 nm and the standard curve was plotted to calculate the protein concentration.

Flow cytometry cell cycle analysis

For cell cycle analysis, the IC50 doses of cancer cells were applied to the cells at a concentration of 300 μ M for 48 h. The cells were then fixed in 70% ethanol, washed with PBS, and stained with PBS containing 20 μ g/ml RNase A and 50 μ g/ml propidium iodide (PI) for 3 h at room temperature. Around 10,000 cells were analyzed by CyAn ADP flow cytometer (Beckman Coulter, Brea, CA, USA) and FCS Express 5 (De Novo Software, Glendale, CA, USA). This experiment was performed two times for symmetric results (Mullen 2004).

Measurements of ROS markers

Malondialdehyde (MDA) measurement

Following the manufacturer's instructions, the MDA content was determined in the cell culture lysate to detect the lipid peroxidation products, using MDA Assay Kit. In this assay, MDA combines with thiobarbituric acid (TBA) to form an adduct. Briefly, cells were homogenized in 300 μ l of the MDA lysis buffer on ice. The samples were centrifuged at 13,000g for 10 min and 200 μ l of the supernatant was placed into a microcentrifuge tube. 600 μ l of the TBA solution was added to each of the standard and sample vials. The vials were then incubated at 95 °C for 60 min then cooled to room temperature in an ice bath for 10 min. 200 μ l from each standard and sample reaction mixture was pipetted into a 96-well plate.

The absorbance was determined by the spectrophotometer (Spectronic, Milton Roy Co.) at 532 nm. After calculating the MDA concentration using dose–response

curve-fitting models (GraphPad, Prism8 software incorporated), the amount of MDA in each sample was obtained from the standard curve (Tsikas 2017).

Nitric oxide (NO) measurement

Nitric oxide content was detected in the culture media of cells by adapting the Miranda et al. method (Miranda et al. 2001). A mixture of 250 ml culture media and 0.5 ml cold absolute ethanol was left for 48 h at 4 °C to reach complete protein precipitation followed by 13,000 rpm centrifugation for 1 h using a cooling centrifuge. In a 96-well microplate, a serial dilution of 100 ml nitrate standard solution was performed in duplicate. Rapidly, 100 ml of vanadium chloride was added to each well followed by 50 ml sulphanilamide and 50 ml *n*-(1-naphthyl) ethylene diamine in 2 N hydrochloric acid and the mixture was incubated for 30 min. Using an ELISA microplate reader (TECAN Sunrise™, Germany), the absorbance at 540 nm was measured and the level of total nitrite/nitrate was revealed and determined using the standard curve.

Reduced glutathione (GSH) measurement

Ellman's method was employed to detect the reduced glutathione content (Ellman 1959). HNO97 and OEC cells were harvested and protein precipitation was done with trichloroacetic acid. The Ellman's reagent [5,5-dithiobis-(2-nitrobenzoic acid)] was added to the supernatant. After the determination of the absorbance at 405 nm using a spectrophotometer (Spectronic, Milton Roy Co.), GSH content was calculated from a standard calibration curve and dose–response curve models (GraphPad, Prism8 software, incorporated).

Statistical analysis

Data were coded and entered using the Graph pad prism 8.0.1 (244) and summarized using mean and standard deviation. Data was double-checked for normality using normality plots and Shapiro Wilk test and proved not to deviate from normal distribution. Comparisons were done using analysis of variance (ANOVA) with multiple comparisons (Tukey) post hoc test. *P* values less than 0.05 were considered statistically significant.

Results

Characterization of AuCh Nps and Cis/AuCh nanocomposite

Ultraviolet–visible (UV–Vis) spectroscopy

The efficiency of cisplatin loading into AuCh Nps conjugates was determined by UV–Vis spectroscopy. The formation of AuCh Nps was exhibited by a peak at a wavelength of 520 nm. Upon the addition of cisplatin, a broadening and red shift in the peak from a wavelength of 520 nm to 530 nm was observed. The plasmon absorption displayed a red shift as the nanoparticle size increased when the different moieties were added (Fig. 1).

Transmission electron microscope (TEM) measurements

The TEM images of AuCh Nps and Cis/AuCh nanocomposite had a spherical shape with uniform size distribution. TEM images of cisplatin loaded on AuCh Nps revealed that the nanocomposite was regularly spherical in shape and had a smooth surface with an increase in the particle size from 12 ± 2 nm to 16 ± 2 nm as indicated by the red shifting

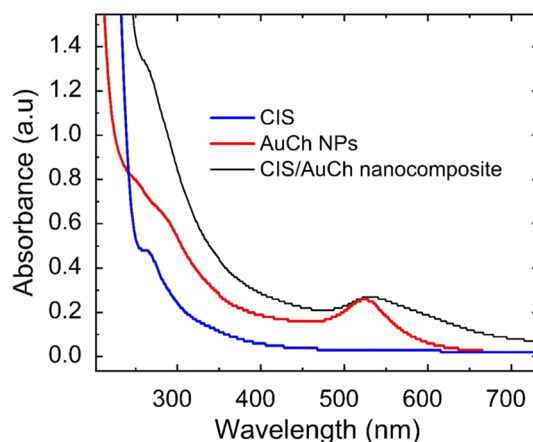


Fig. 1 Absorption spectra of Cis (cisplatin), AuCh Nps, and Cis/AuCh nanocomposite

in the plasmon absorption band that shifted toward a longer wavelength. Here the plasmon coupling obviously appeared with linearly arranged coupled particles confirming the nanocomposite formation (Fig. 2).

Dynamic light scattering (DLS) analysis and zeta potential

For proper study of the hydrodynamic diameter and surface charge of the synthesized colloidal AuCh Nps and Cis/AuCh nanocomposite, DLS and zeta potential measurements were performed. Cisplatin-loaded AuCh Nps revealed a high zeta potential along with small uniform particles. AuCh Nps and Cis/AuCh nanocomposite hydrodynamic sizes were 101.3 and 146.2 nm, respectively (Fig. 3), with zeta potentials of 36.6 and 39.3 mV (Fig. 4).

Fourier transform infrared spectroscopy (FT-IR) analysis

An FT-IR analysis was employed to confirm the interactions between AuCh Nps and cisplatin. The chemical interactions resulting from mixing two or more components would trigger a change or shift in the characteristic peaks. From FT-IR analysis of cisplatin solution, the main characteristic peaks appeared at 3434.6 cm^{-1} besides stretching vibration in the range from 577.57 to 624.19 cm^{-1} , and peaks at 1425.14 and 1630.52 cm^{-1} . As shown in (Fig. 5), AuCh Nps exhibited characteristic peaks at 3427.85 cm^{-1} , and upon loading cisplatin, the peak showed a slight red shift to 3030.74 cm^{-1} . A peak at 1568.81 cm^{-1} was also detected. In addition, bands at 1413 cm^{-1} and 1258 cm^{-1} were observed. In the case of Cis/AuCh nanocomposite, there was an intensity reduction of all bands and NH which broadened and minimally shifted to lower wavelengths at 3430 cm^{-1} . Cis/AuCh nanocomposite exhibited a blue shift of the O–H in-plane bending from 1425 to 1414 cm^{-1} .

X-ray diffraction (XRD) analysis

The crystalline property of nanoparticles and nanocomposites is one of the crucial elements affecting their mechanical characteristics. Sharp peaks were obvious at $2\theta = 27, 30.1, 36.7, 44.1, 48.5$ and 57 degrees. The 112, 220, and 116 diffraction line characteristics of chalcopyrite structure were also observed (Fig. 6A). The XRD

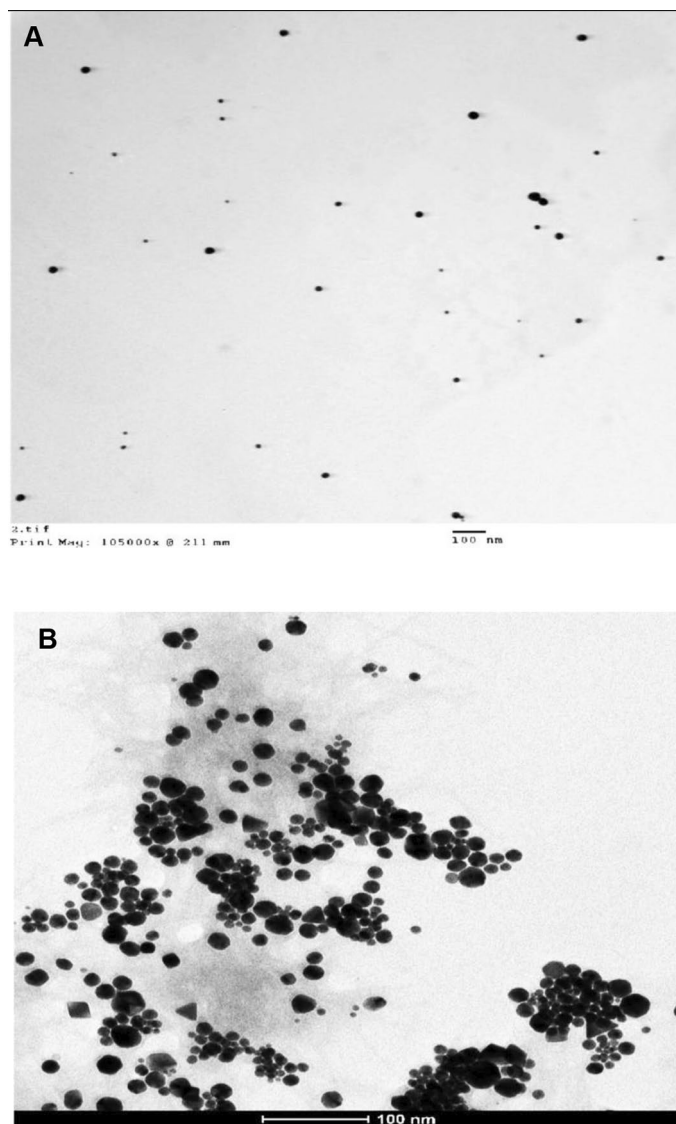


Fig. 2 TEM images of (A) AuCh Nps and (B) Cis/AuCh nanocomposite (magnification 100 nm)

pattern of AuCh Nps showed characteristic diffraction peaks at 37.97° , 44.18° , 64.62° , and 77.45° , corresponding to (111), (200), (220), and (311) (Fig. 6B). The characteristic peaks of AuCh Nps were observed to shift and at very low intensity. The Cis/AuCh nanocomposite sample showed sharp peaks at $2\theta = 19.92^\circ, 27^\circ, 30.1^\circ, 36.7^\circ, 44.1^\circ, 48.5^\circ$ and 57° corresponding to the Cis/AuCh (Fig. 6C).

Assessment of cytotoxicity

The results of the SRB cytotoxicity assay revealed that the IC₅₀ doses after 48 h treatment with cisplatin, AuCh Nps, and Cis/AuCh nanocomposite on OSCC (HNO97) cell line were (11.5 $\mu\text{g/ml}$, 12.5 $\mu\text{g/ml}$, 6.2 $\mu\text{g/ml}$, respectively) (Fig. 7A) and on normal OEC cell line were (20 $\mu\text{g/ml}$, 40 $\mu\text{g/ml}$ and 44.5 $\mu\text{g/ml}$, respectively) (Fig. 7B).

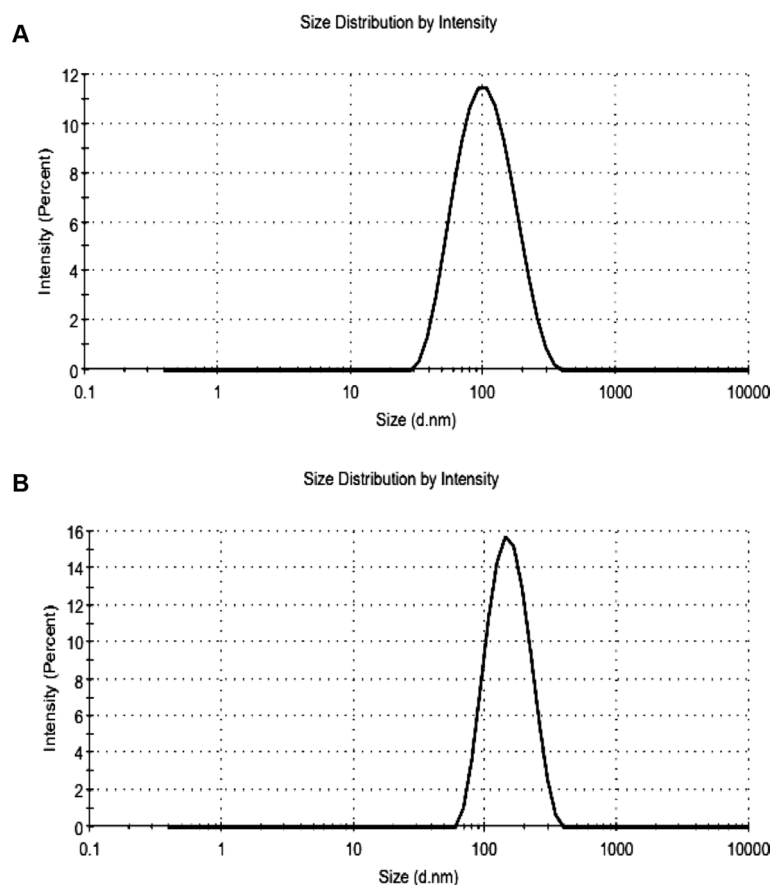


Fig. 3 Particle size of (A) AuCh Nps and (B) Cis/AuCh nanocomposite

Microscopic morphological changes

Microscopic examination revealed that the control untreated HNO97 and OEC cells were viable and confluent. The cells incubated with the HNO97–IC50 doses of cisplatin, AuCh Nps, and Cis/AuCh nanocomposite lost their adhesion and showed apoptotic cellular changes of cellular and nuclear shrinkage, membrane blebbing, peripheral chromatin condensation, chromatin fragmentation, and apoptotic bodies. AuCh Nps and Cis/AuCh nanocomposite-treated OEC groups revealed more confluent attached areas and less obvious apoptotic cells (Fig. 8).

Caspase 3 immunohistochemical results and apoptotic index (AI)

After incubation with the 48 h-HNO97–IC50 doses, Caspase 3-immunopositive cells revealed cytoplasmic staining besides nuclear staining in some cells. Many immunostained apoptotic bodies were also detected (Fig. 9). The Caspase 3-AI showed a statistically significant increase in all treated groups in comparison to the untreated control ($P=0.001$) in the HNO97 cell line, where the Cis/AuCh nanocomposite-treated group presented the highest value. On the other hand, regarding OEC cell line, only the cisplatin-treated group revealed a statistically significant increase in AI from the control ($P=0.001$) (Fig. 10).

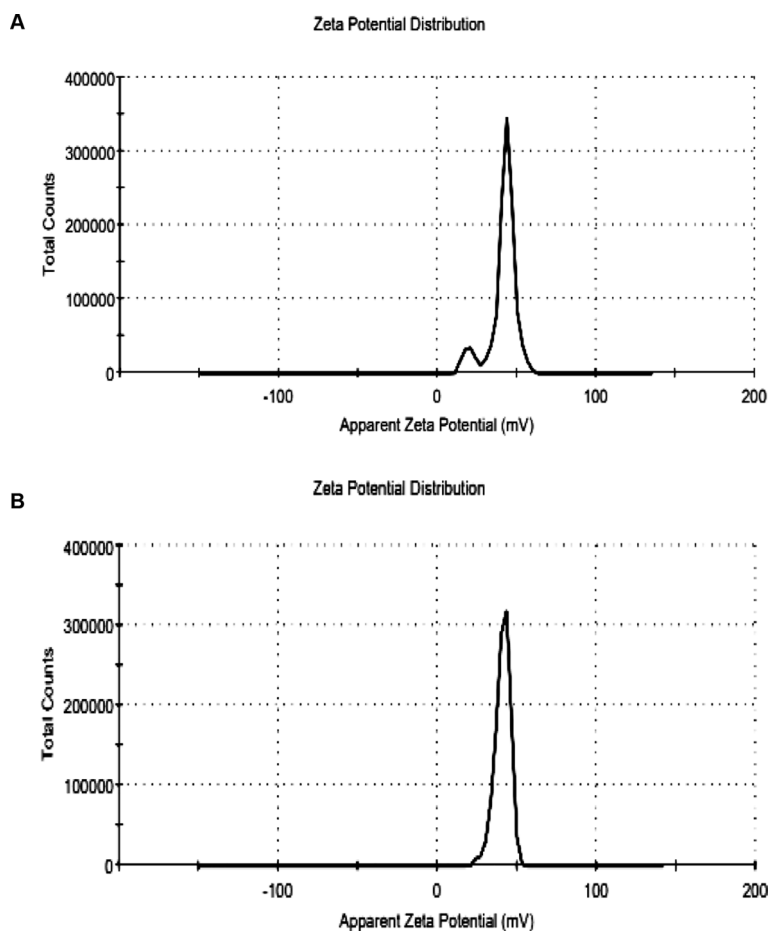


Fig. 4 Zeta potential of (A) AuCh Nps and (B) Cis/AuCh nanocomposite

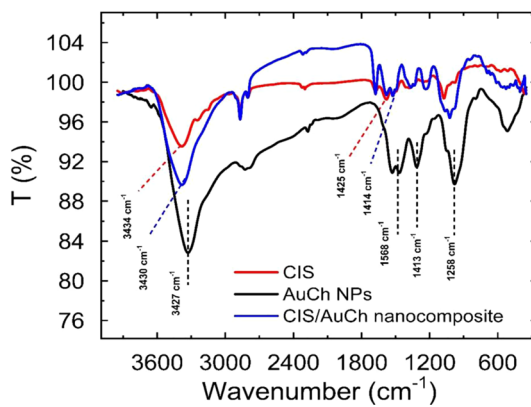


Fig. 5 FT-IR spectra of Cis (Cisplatin), AuCh Nps, and Cis/AuCh nanocomposite

Enzyme-linked immunosorbent assay (ELISA) measurements of apoptotic proteins levels

Regarding the HNO97 cell line, the protein levels of the pro-apoptotic markers increased significantly in all treated groups compared to the control untreated one, while the anti-apoptotic marker (Bcl-2) decreased significantly. The Cis/AuCh nanocomposite-treated

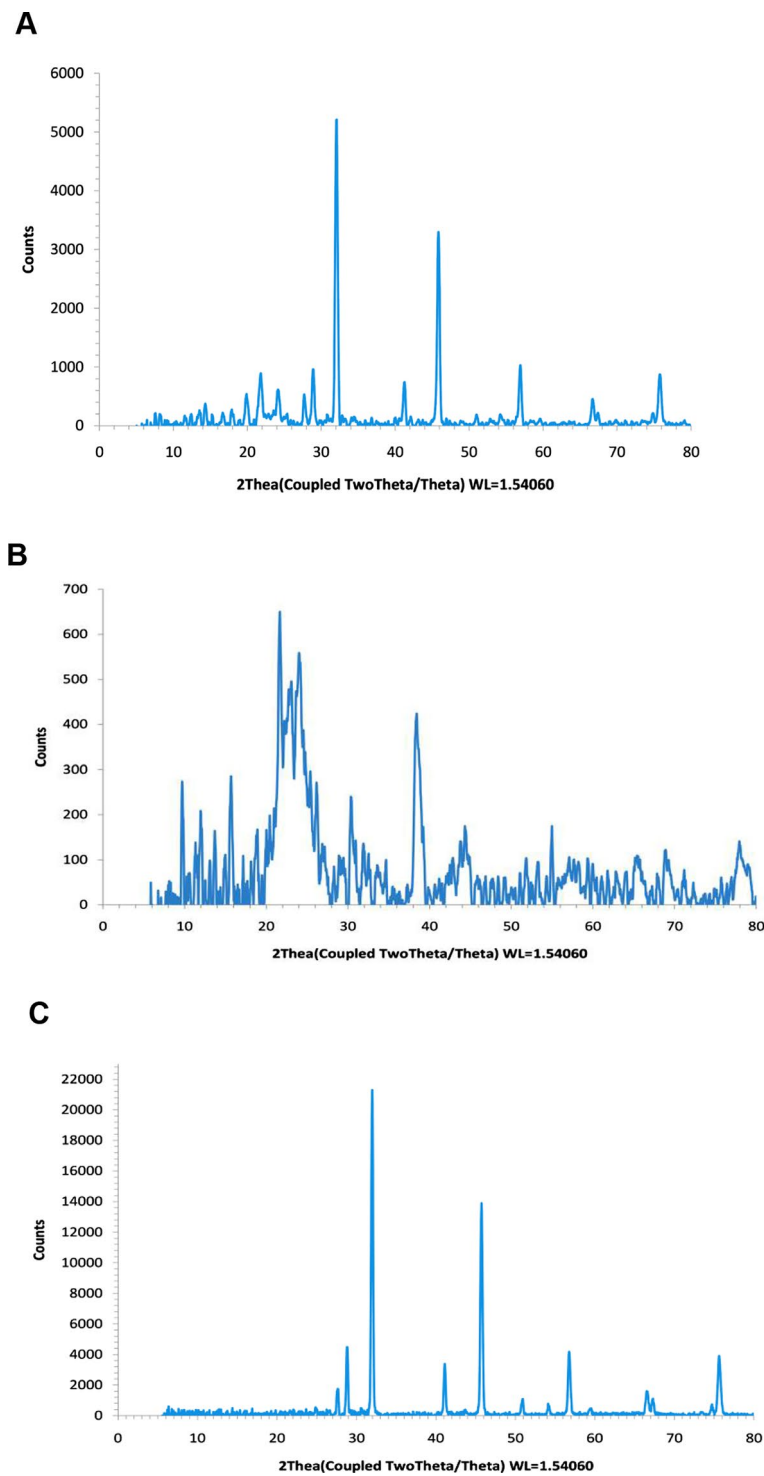


Fig. 6 X-ray diffraction (XRD) patterns of (A) Cis (Cisplatin), (B) AuCh Nps, (C) Cis/AuCh nanocomposite

cells presented a significant rise in the level of the pro-apoptotic markers; P53, Caspase 3, Caspase 8, and Bax, besides a significant drop of Bcl-2 level compared to cisplatin ($P=0.0016$, 0.0427 , 0.0161 , <0.0001 , and 0.0096 , respectively) and AuCh Nps ($P=0.0001$, 0.0011 , 0.0001 , <0.0001 , and 0.0003 , respectively) treated cells. In addition,

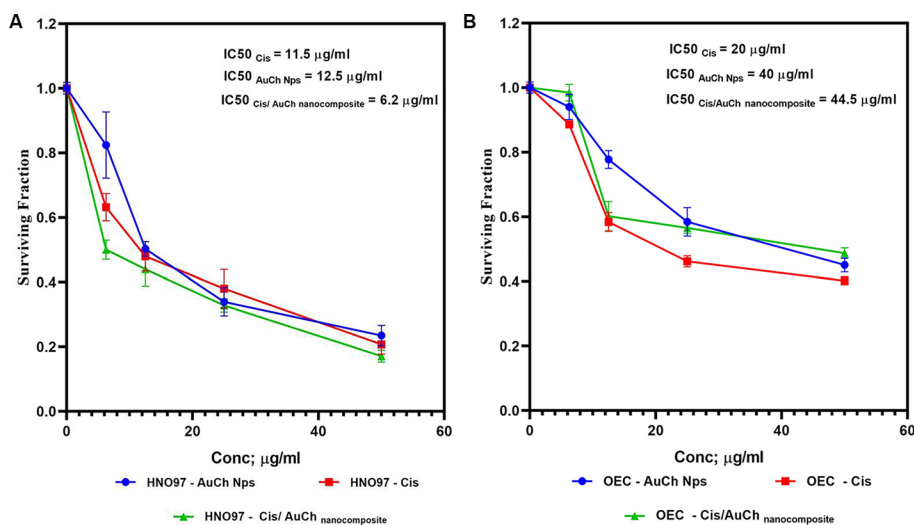


Fig. 7 Line charts representing the IC50 after 48 h treatment with Cis (Cisplatin), AuCh Nps, and Cis/AuCh nanocomposite on (A) HNO97 cell line and (B) OEC cell line

the AuCh Nps group presented a significantly lower level of the pro-apoptotic markers and a higher level of Bcl-2 in comparison to the cells treated with cisplatin (Fig. 11).

On the other hand, there was an increase in the pro-apoptotic markers and a reduction in the protein level of Bcl-2 in all treated groups relevant to the untreated control in the OEC cell line; however, this effect was insignificant as regards P53, Caspase 3, and Caspase 8 in Cis/AuCh nanocomposite treated cells. The levels of P53, Caspase 3, Caspase 8 and Bax were lower in AuCh Nps ($P=0.0028$, 0.0016 , 0.0614 , and 0.0385 , respectively) and Cis/AuCh nanocomposite ($P=0.0011$, 0.0008 , 0.029 , and 0.1273 , respectively) treated cells in comparison to the cisplatin-treated group, while the level of Bcl-2 was higher in AuCh Nps ($P=0.0862$), and Cis/AuCh nanocomposite ($P=0.0357$) than cisplatin. No significant difference in the levels of all protein markers was detected between AuCh Nps and Cis/AuCh nanocomposite-treated groups in OEC (Fig. 12).

Cell cycle analysis by flow cytometry

Analysis of the cell cycle by flow cytometry of the HNO97 cell line showed that most of the untreated cells were in G0/G1 phase (78.595%), with S phase (18.835%) and G2/M phase (2.745%). After treatment with the IC50, most of the cisplatin-treated cells shifted to the S phase (70.165%) with an increase in the mean percentage of cells in the G2/M phase to (4.765%). In the AuCh Nps group, the S phase population increased to (33.57%), while the G2/M phase decreased to (0.34%). Cis/AuCh nanocomposite showed S phase shift to (35.765%) (Fig. 13).

Regarding the OEC cell line, the cisplatin-treated group revealed the most shifts from the control. The cells shifted from the G0/G1 phase to the S phase (58.455%) and G2/M (14%). AuCh NPs and Cis/AuCh nanocomposite showed S phase cell shift to 48.325% and 46.115%, respectively, and G2/M shift to 4.89% and 7.78%, respectively (Fig. 14).

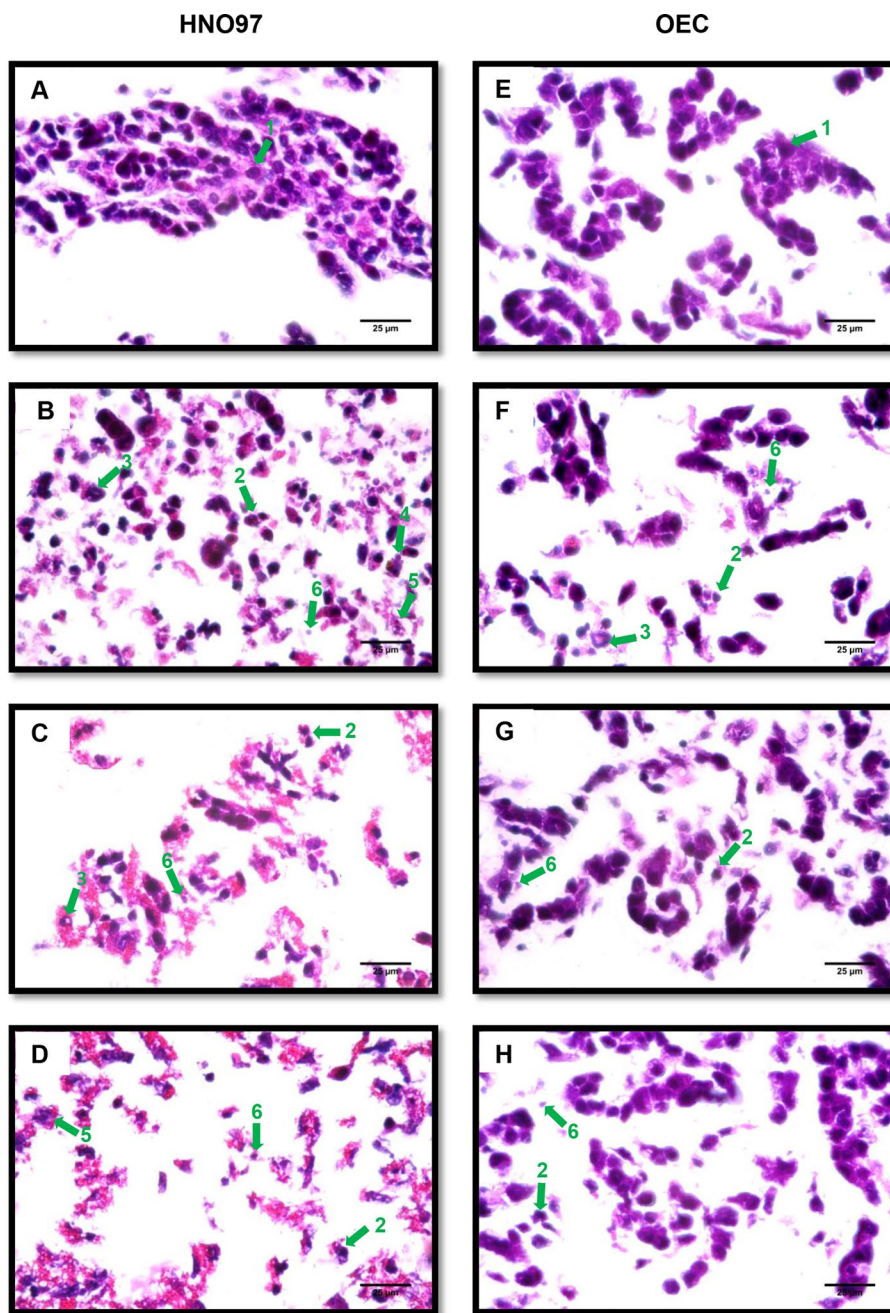


Fig. 8 Photomicrographs showing morphological apoptotic changes of HNO97 and OEC treated groups. **A, E** Control untreated groups, **B, F** Cisplatin-treated groups, **(C, G)** Auch Nps-treated groups, **(D, H)** Cis/AuCh nanocomposite-treated groups. The numbers indicate examples of the morphological features of the stained cells as follows: 1: confluent viable cells, 2: apoptotic shrunken cells with a shrunken nucleus, 3: peripheral chromatin condensation, 4: membrane blebbing, 5: fragmentation of chromatin, 6: apoptotic bodies (**H & E**, 1000X, Oil)

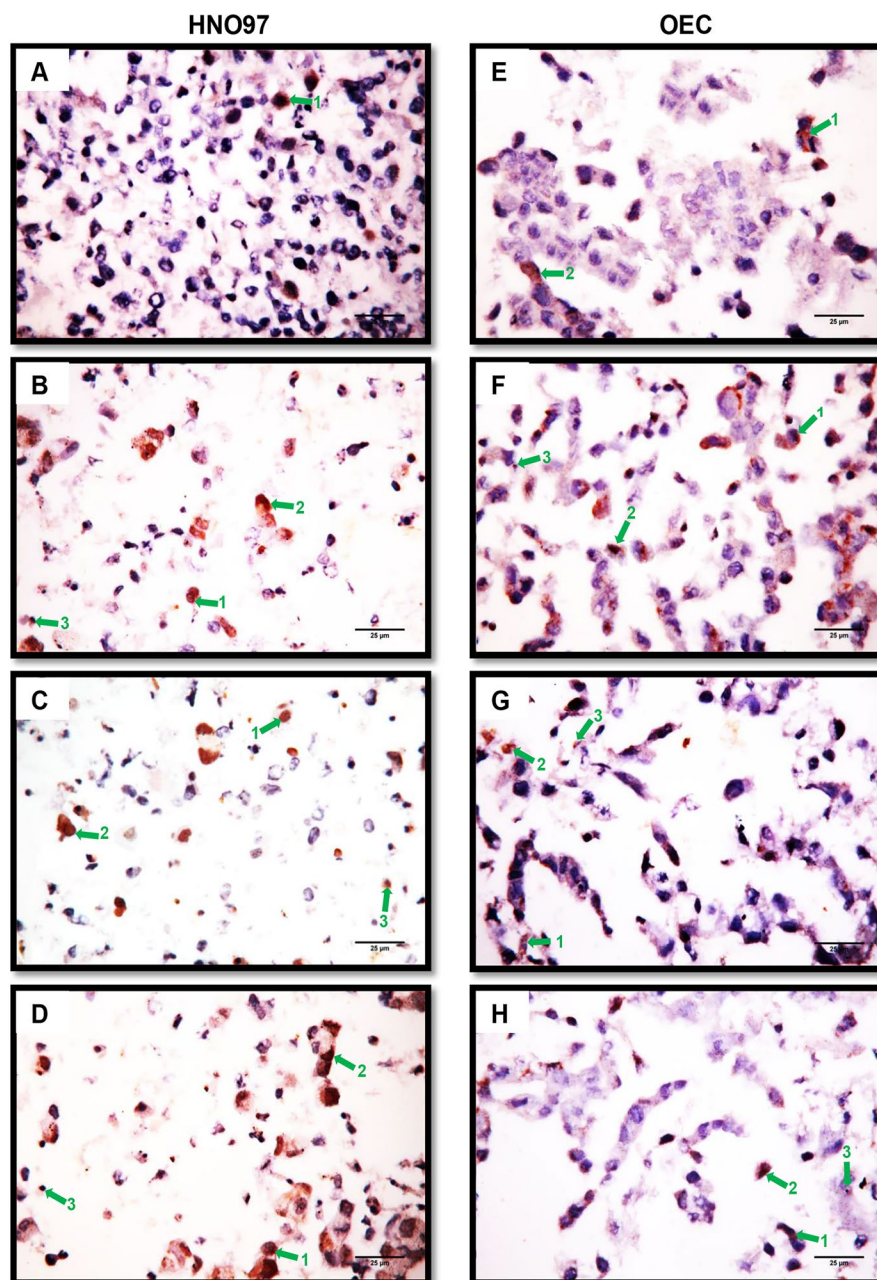


Fig. 9 Photomicrographs showing positive immunoreactivity of the apoptotic cells in HNO97 and OEC groups. **A, E** Control untreated groups. **B, F** Cisplatin-treated groups, **(C, G)** Auch Nps-treated groups, **(D, H)** Cis/AuCh nanocomposite-treated groups. The numbers indicate the location of the immuno-reaction as follows: 1: Cytoplasmic, 2: Nuclear, 3: Apoptotic bodies (anti-Caspase 3, 1000X, Oil)

Evaluation of reactive oxygen species (ROS)

All HNO97 treated groups revealed a statistically significant increase in the expression of MDA and NO from the control untreated cells and a significant reduction in GSH. The highest MDA and NO, and the lowest GSH expressions were detected in the Cis/AuCh nanocomposite ($P=0.006, <0.001$, and 0.001 , respectively) (Fig. 15A–C).

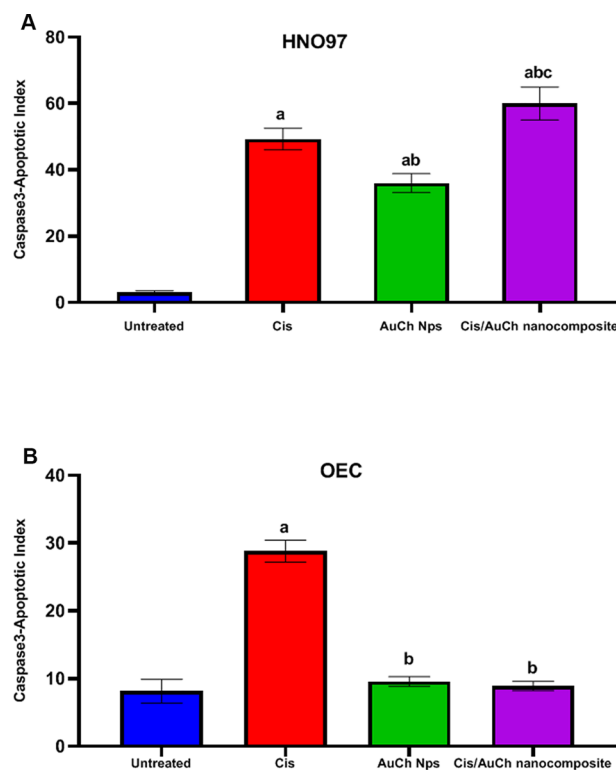


Fig. 10 Bar charts representing the effect of Cis (Cisplatin), AuCh Nps, Cis/AuCh nanocomposite on Caspase 3-apoptotic index (AI) in **(A)** HNO97 and **(B)** OEC cell lines. "a" indicates the significance compared to untreated group, "b" to Cis and "c" to Auch Nps ($p < 0.05$)

Conversely, only the cisplatin-treated group in the OEC cell line showed a statistically significant rise in MDA and NO and a reduction in GSH (Fig. 15D–F).

Discussion

Cisplatin is the primary chemotherapeutic agent for OSCC treatment. However, this anticancer effect is associated with high multisystem toxicity (Cheng et al. 2021b). Thus, it is inevitable to seek alternatives with fewer side effects.

In this study, UV–Vis spectroscopy results of the synthesized nanoparticles revealed that AuCh Nps formation by a peak at a wavelength of 520 nm indicates a successful functionalization with cisplatin, while the broadening and red shift in the peak from a wavelength of 520 nm to 530 nm after addition of cisplatin denotes a successful conjugation of cisplatin to AuCh Nps (Khamaikawin and Locharoenrat 2023).

Regarding the zeta potential, our results revealed that AuCh Nps and Cis/AuCh nanocomposite possessed a high potential and a small size of their particles. The high zeta potential is associated with a large repulsive force between the nanoparticles and consequently high stability. Moreover, the charge density of the particles significantly affects their adherence with the negatively charged cancer cell membrane, thus influencing the stability and drug release. Accordingly, it was recommended to use positively charged nanoparticles as carriers for drug delivery. The electrostatic

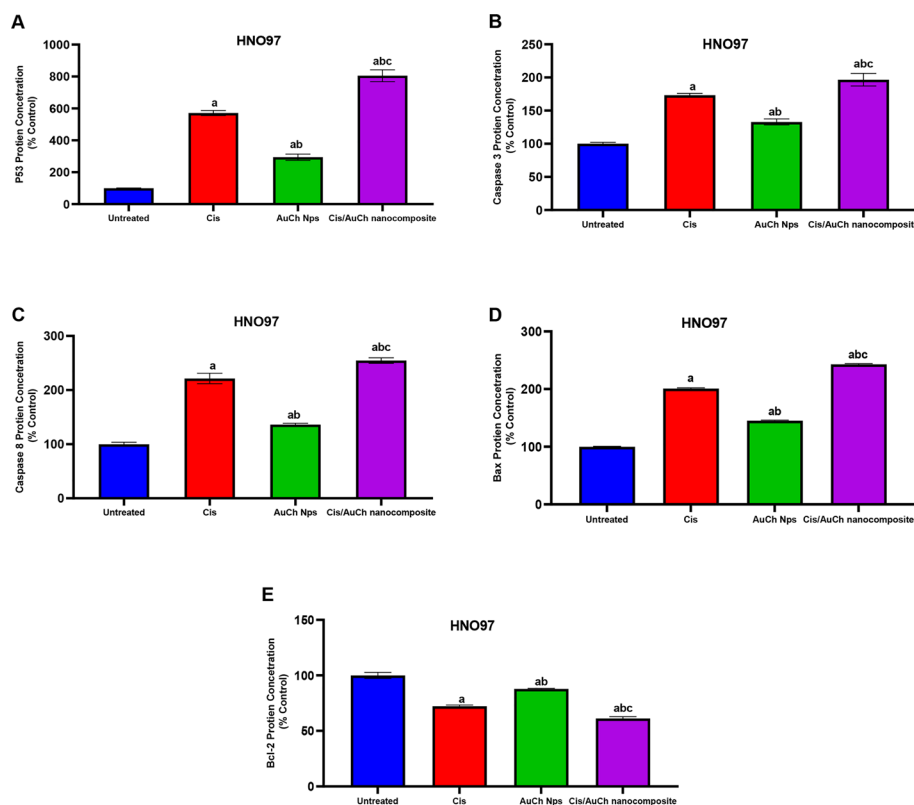


Fig. 11 Bar charts representing the effect of Cis (Cisplatin), AuCh Nps, Cis/AuCh nanocomposite on the protein levels of the pro-apoptotic markers; **(A)** P53, **(B)** Caspase 3, **(C)** Caspase 8, **(D)** Bax, and the anti-apoptotic marker **(E)** Bcl-2 in HNO97 cells. “a” indicates the significance compared to untreated group, “b” to Cis and “c” to Auch Nps ($p < 0.05$)

repulsions usually inhibit the aggregation of the charged particles with an ideal zeta potential ≥ 30 mV (Ramadan et al. 2022; Faïd et al. 2023; Mohamad et al. 2023; Alex-eree et al. 2024).

From the FT-IR analysis of cisplatin solution, the main peak appeared at 3434.6 cm^{-1} was due to $-\text{NH}$ stretching and the stretching vibration in the range from 577.57 cm^{-1} to 624.19 cm^{-1} was due to Pt–O–Pt linkage (Shaaban et al. 2022; Ramadan et al. 2024a). Peaks at 1425.14 and 1630.52 cm^{-1} corresponded to HNH asymmetric and symmetric bending, respectively.

AuCh Nps exhibited characteristic peaks at 3427.85 cm^{-1} which were attributed to hydrogen-bonded O–H stretching vibration bands of N–H stretching from primary amine and type II amide which were overlapped in the same region upon loading cisplatin. This peak showed a slight red shift to 3030.74 cm^{-1} (Faïd et al. 2023, 2024). The peak at 1568.81 cm^{-1} corresponded to C–O stretching along with N–H deformation mode (Regiel-Futyra et al. 2015). The band at 1413 cm^{-1} was attributed to bending vibration of OH group, while the band at 1258 cm^{-1} corresponded to the amide III vibration mode due to the combination of N–H deformation and C–N stretching (Faïd et al. 2023, 2024). The blue shift of the O–H in-plane bending from 1425 to 1414 cm^{-1} of Cis/AuCh nanocomposite could be due to loading cisplatin on

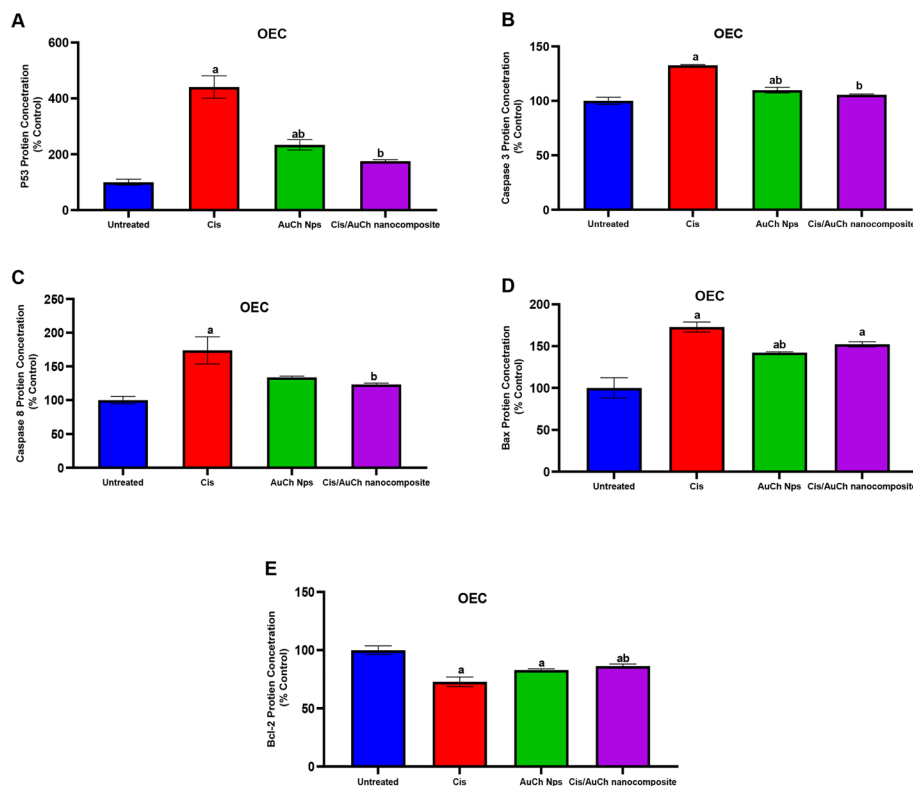


Fig. 12 Bar charts representing the effect of Cis (Cisplatin), AuCh Nps, Cis/AuCh nanocomposite on the protein levels of the pro-apoptotic markers; **(A)** P53, **(B)** Caspase 3, **(C)** Caspase 8, **(D)** Bax, and the anti-apoptotic marker **(E)** Bcl-2 in OEC cell line. "a" indicates the significance compared to untreated group, "b" to Cis and "c" to AuCh Nps ($p < 0.05$)

AuCh Nps. The slight change in the partial peaks indicates the formation of bonding between cisplatin and AuCh Nps.

XRD is the method usually used to determine the crystallinity, phase behavior, and lattice constants. The sharp peaks that appeared at $2\theta = 27, 30.1, 36.7, 44.1, 48.5,$ and 57 degrees, were due to the platinum in the cisplatin. The three diffraction peaks at the 2θ values of $27, 44.1,$ and 57 were associated with the (112), (220), and (116) reflections of the chalcopyrite cisplatin, respectively (Jayasuriya and Darr 2013). Regarding AuCh Nps, Bragg's reflection is in good agreement with the face-centered cubic (FCC) structure of AuCh Nps (JCPDS card no: 04-0784). In addition, the most prominent diffraction peak at 22.8° confirmed the crystalline structure of chitosan (Dananjaya et al. 2017). Our XRD results of AuCh Nps agree with the previous findings of Kanwal et al. (2019), Saravanakumar et al. (2020), and Salah et al. (2023).

The characteristic peaks of AuCh Nps were observed to shift at a very low intensity as they were loaded and covered with cisplatin (Pucelik et al. 2022). This overlapping between the peaks indicates the loading and formation of a new crystalline nature of the Cis/AuCh nanocomposite. The sharp peaks at $2\theta = 19.92^\circ, 27^\circ, 30.1^\circ, 36.7^\circ, 44.1^\circ, 48.5^\circ$ and 57° of Cis/AuCh nanocomposite sample corresponded to the Cis/AuCh. Thus, these results verify the successful loading of cisplatin into AuCh Nps.

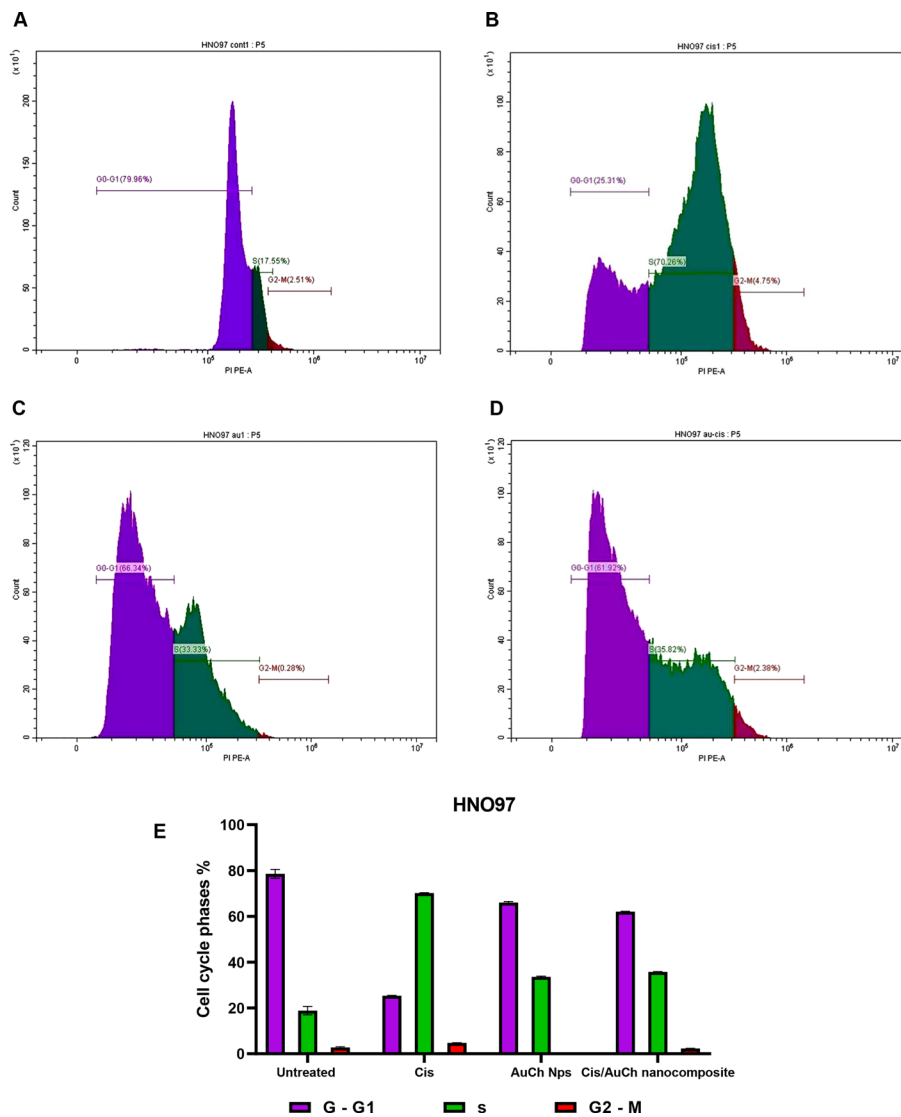


Fig. 13 Cell cycle changes on HNO97 cells after treatment with Cis (Cisplatin), AuCh Nps, and Cis/AuCh nanocomposite

Our study revealed that conjugating cisplatin with AuCh Nps reduced the IC50 dose after 48 h from 11.5 $\mu\text{g/ml}$ to 6.2 $\mu\text{g/ml}$. In addition, AuCh Nps alone were cytotoxic to the HNO97 cell line with IC50 of 12.5 $\mu\text{g/ml}$. These findings are parallel with Dhar et al. (2009), Brown et al. (2010), and Ganji et al. (2021), who found that binding platinum-based chemotherapeutic drugs to AuNps was more effective and more cytotoxic than their free state on several cancer cell lines. In addition, niosomes containing a chemotherapeutic drug and AuNps coated with chitosan revealed a significant cytotoxic effect on breast cancer cells (Zenjanab et al. 2024). On the other hand, the cytotoxic effect of Cis/AuCh nanocomposite on the OEC cell line was much lesser than that of cisplatin with IC50 of 44.5 $\mu\text{g/ml}$. Thus, for proper exploration of the antitumor effect and safety of the study therapeutic agents, the IC50 doses of HNO97 cell line were chosen for detecting the changes in cytological morphology, apoptotic

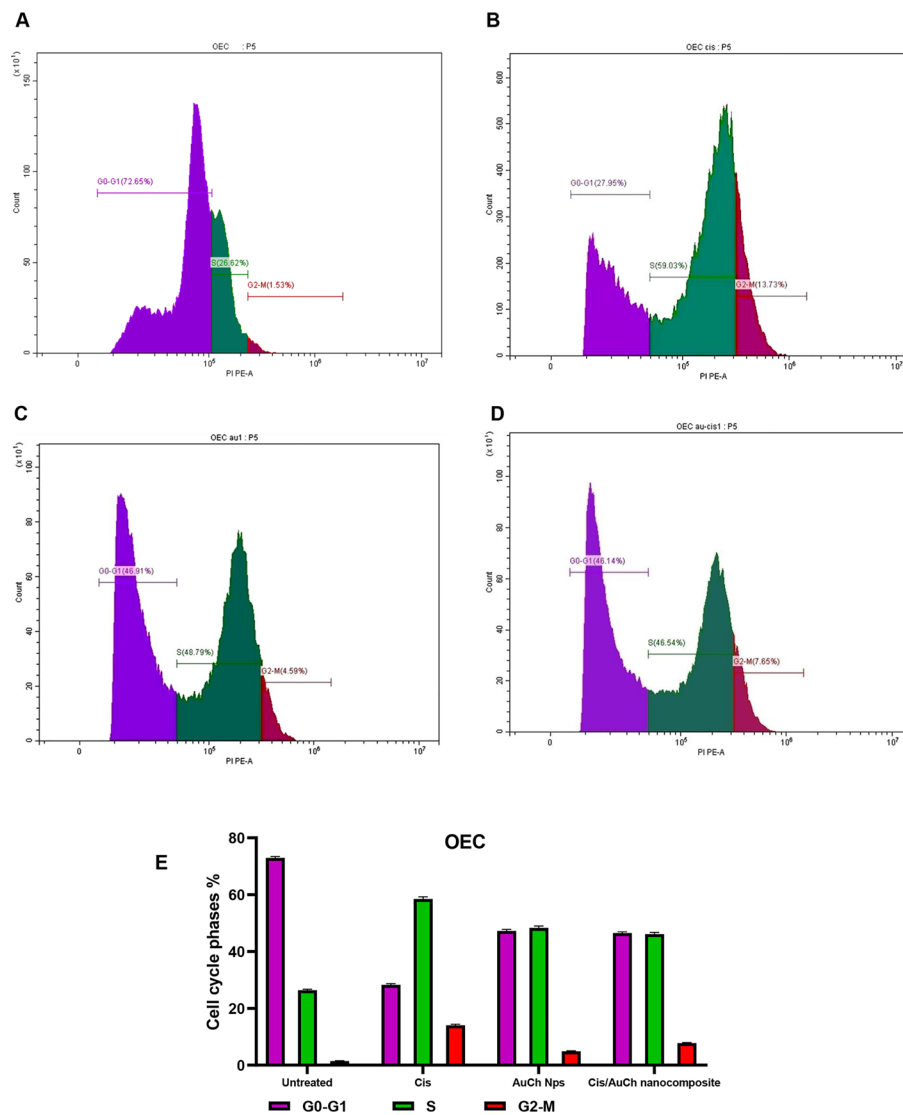


Fig. 14 Cell cycle changes on OEC cell line after treatment with Cis (Cisplatin), AuCh Nps, and Cis/AuCh nanocomposite

index, apoptotic protein levels, cell cycle, and ROS markers in both HNO97 and OEC cell lines.

Besides the obvious apoptotic microscopic features observed on applying the 48 h-IC50 doses of AuCh Nps and Cis/AuCh nanocomposite on HNO97 cells, Caspase 3 immunohistochemical staining revealed positive cytoplasmic and nuclear staining in the apoptotic cells besides some morphologically appearing healthy cells which was also the case in all study groups. This was attributed to the ability of the Caspase 3 marker to detect apoptosis in the very early stage. Staining of the nucleus could be explained by the nuclear translocation of the protein (Bressenot et al. 2009). AI results presented a significant rise in the number of apoptotic cells compared to the control, on contrary to OEC which did not show any significant difference with the untreated group. Moreover, ELISA results of HNO97 cell line displayed a significant increase in the protein levels, of

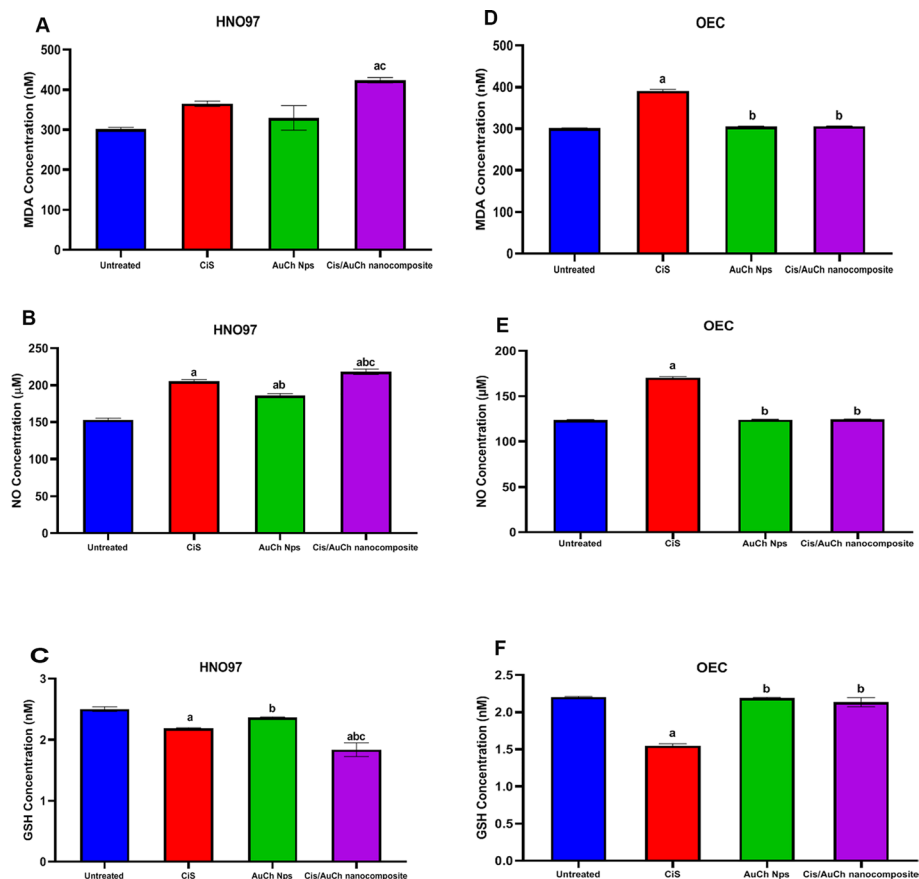


Fig. 15 Bar charts representing the effect of Cis (Cisplatin), AuCh Nps, Cis/AuCh nanocomposite on the levels of ROS markers in HNO97 and OEC cell lines; **(A, D)** MDA, **(B, E)** NO, and **(C, F)** GSH. “a” indicates the significance compared to untreated group, “b” to Cis and “c” to Auch Nps ($p < 0.05$)

the pro-apoptotic markers of the intrinsic pathway Bax and caspase 3, along with a significant decrease in the level of anti-apoptotic Bcl-2 protein.

Similar to our results, Bandyopadhyay et al. (2021) detected nuclear fragmentation of breast cancer cells after exposure to 1/3 IC50 of chitosan-functionalized AuNps. In addition, it was reported that niosomes formed by chitosan coated chemotherapeutic agents and AuNps remarkably increased the apoptotic rate of breast cancer cells after 48 h (Zenjanab et al. 2024). Furthermore, AuCh Nps proved to be effective in inducing the intrinsic pathway of apoptosis in HeLa cells, a finding detected by caspase 3 activation (Martínez-Torres et al. 2018). Another study on breast cancer showed a rise in Bax/Bcl-2 ratio, forming mitochondrial membrane pores, and activation of the initiator and executioner caspases (Bandyopadhyay et al. 2021). Caspase 8, the enzyme responsible for the extrinsic apoptotic pathway was found elevated in all treated groups. Although Bandyopadhyay et al. (2021) did not detect any effect of AuCh Nps on the extrinsic pathway of apoptosis in breast cancer cells, previous studies reported that both chitosan and AuNps were effective in inducing Caspase 8 in cancer cell lines (Takimoto et al. 2004; Choi et al. 2012; Doghish et al. 2022). P53 “cell cycle checkpoint and tumor suppressor protein” was elevated in our study following Selim and Hendi (2012), who observed an increase in P53 fold change after treating the MCF-7 cell line with AuNps.

Cell viability inhibition can be related to the induction of cell cycle arrest. Our study detected cell cycle arrest at the S phase by AuCh Nps and Cis/AuCh nanocomposite on the HNO97 cell line. Although similar arrest at the S phase and mild G2/M were detected in the OEC cell line, the effect of AuCh Nps and Cis/AuCh nanocomposite on normal cell lines was much milder than that of cisplatin. The S phase is the stage before cell division during which DNA synthesis takes place, while G2/M is the checkpoint before mitosis progression, thus blockage of some cells at these phases prevents them from entering mitotic cell division (Kubo et al. 2003; Luk et al. 2005). P53 can sustain S and G2 arrest followed by activating apoptosis-related genes (Agarwal et al. 1998; Luk et al. 2005). P53-mediated G2 arrest may be achieved through the induction of p21 and 14-3-3 σ , the G2/M progression inhibitors, while S phase arrest could be p21 independent (Hermeking et al. 1997; Agarwal et al. 1998; Bunz et al. 1998; Luk et al. 2005). Previously, AuNPs were said to arrest breast cancer cells at the G2/M phase (Abdel-Ghany et al. 2020), while Choi et al. (2012) detected the arrest in the sub-G1 phase in lung adenocarcinoma cells. In addition, chitosan efficiently arrested the cell cycle at the G1 and S phases when applied to Ca9-22 oral cancer cells (Wimardhani et al. 2014).

It was demonstrated earlier that AuCh Nps and other AuNps were able to induce cancer cell death by ROS production (Chompoosor et al. 2010; Boyles et al. 2015; Martínez-Torres et al. 2018). Our results revealed high MDA and NO and low GSH expressions in HNO97 cells treated with AuCh Nps and Cis/AuCh nanocomposite. ROS production by nanoparticles can cause mitochondrial alterations leading to apoptosis (Liu et al. 2013). Lipid peroxidation and excessive MDA production indicate ROS tissue damage (Gawel et al. 2004). NO can cause damage to DNA and P53 activation leading to upregulation of the extrinsic apoptotic pathway (Kannappan et al. 2010), or upregulation of Bax stimulating the intrinsic apoptotic pathway (Park et al. 2013). Moreover, the exhaustion of the GSH antioxidant capacity of cells by high ROS release finally leads to apoptosis (Li et al. 2021). Conversely, the used doses did not cause a noticeable rise in ROS markers in the OEC cell line. This is in accordance with Lorenzo-Anota et al. (2021), who detected low ROS production and low cell death in non-cancer cells.

A significant increase in Caspase 3-AI, besides the upregulation of the intrinsic and extrinsic pro-apoptotic proteins, and downregulation of Bcl-2 in the HNO97 cell line by the Cis/AuCh nanocomposite compared to the cisplatin-treated group were obvious in this study. However, these apoptotic effects were significantly lower than the cisplatin-treated group in the OEC cell line. Apoptosis induction, cell cycle arrest, and ROS production are well-established mechanisms by which cisplatin acts effectively to destroy oral cancer cells (Sancho-Martínez et al. 2012; Cheng et al. 2021b). Although Cis/AuCh nanocomposite caused cell cycle arrest at the S phase in HNO97 cells, the cisplatin-treated group caused a more significant shift in the cell cycle. This indicates that the superiority of the apoptotic effect of Cis/AuCh nanocomposite on HNO97 cells was at the first place due to more ROS production rather than more cell cycle changes. The conjugation of cisplatin with AuCh Nps gave an additive benefit in eradicating oral cancer cells by adding pro-apoptotic and ROS-producing properties of both gold and chitosan. In addition, using chitosan as a reducing and capping agent increases the muco-adhesion properties of the particles to the cell membrane and enhances more diffusion of cisplatin (Gulati et al. 2021).

The safety of the newly formulated Cis/AuCh nanocomposite on OEC, is said to be related to the lower cisplatin amount used and the cancer cell selectivity of AuCh Nps regarding ROS production (Lorenzo-Anota et al. 2021). In addition, Martínez-Torres et al. (2019) supposed that AuCh Nps activate different mechanisms for selective cytotoxicity against cancer cells without affecting the normal ones. Furthermore, chitosan and chitosan-based chemotherapeutic drug delivery systems were reported to have an affinity for Mucin1 receptors which are overexpressed on cancerous cells providing a preferential drug delivery and more intracellular and extracellular accumulation to cancer cells over normal cells (Wiranowska et al. 2020).

This work paves the way for further studies to detect the effect of Cis/AuCh nanocomposite in different oral cancer cell lines and normal cell lines. In addition, it is inevitable to further explore the effect of the nanocomposite on different OSCC carcinogenic pathways. Animal studies and clinical trials will be the next step to unveil the interaction of Cis/AuCh nanocomposite with tumor microenvironment and explore their effect on metastatic models. Previously, it was found that the gold nano-delivery system acts its anticancer role by reprogramming the tumor microenvironment (Saha et al. 2016). Designing a proper clinical trial study will be the next challenge to examine any immune reaction against the nanocomposite.

AuNps were proven excellent carriers of the chemotherapeutic drugs in targeted drug delivery system (Nejati et al. 2022). Especially those capped and reduced by chitosan have higher stability, more selectivity to cancer cells, and increased safety on normal cells, removing the fear of long-term retention of AuNps in the body (Gulati et al. 2021). Moreover, the size of our prepared Cis/AuCh nanocomposite is considered optimal for penetrating tumor tissue and capillaries (Kenchegowda et al. 2021). Thus, it is predicted to greatly enhance the biodistribution of cisplatin and reduce its systemic toxicity in OSCC patients.

Conclusion

Cis/AuCh nanocomposite represents a promising therapeutic agent for the treatment of OSCC. It proved effective in inducing apoptosis, cell cycle arrest, and ROS production in HNO97 cell line while being safer than cisplatin on normal OEC cell line.

Abbreviations

OSCC	Oral squamous cell carcinoma
ROS	Reactive oxygen species
AuNps	Gold nanoparticles
AuCh Nps	Chitosan-reduced gold nanoparticles
Cis/AuCh nanocomposite	Cisplatin-loaded chitosan gold nanoparticles
OEC	Oral epithelial cells
UV-Vis	Ultraviolet-visible
TEM	Transmission electron microscope
DLS	Dynamic light scattering
FT-IR	Fourier Transform Infrared Spectroscopy
XRD	X-ray diffraction
DMEM	Dulbecco's modified eagle medium
Pen-Strep	Penicillin-streptomycin
HFBS	Heat-inactivated fetal bovine serum
SRB	Sulforhodamine B
MDA	Malondialdehyde
GSH	Reduced glutathione
ELISA	Enzyme-linked immunosorbent assay
O.D.	Optical density

H & E	Hematoxylin and eosin
PBS	Phosphate-buffered saline
IHC	Immunohistochemical
PBS-T	Phosphate-buffered saline with Tween 20
HRP	Horseradish peroxidase
DAB	Diaminobenzidine
AI	Apoptotic index
PI	Propidium iodide
TBA	Thiobarbituric acid
NO	Nitric oxide

Acknowledgements

Not applicable.

Author contributions

BA, RM, and MM: planning, capturing the cytological photos, formal analysis, interpretation of data, writing the cytological morphological changes results, writing and revising the manuscript in consultation with MS, MR and AF; MS: planning, providing cell lines, performing cell culturing, cytotoxicity and ROS analysis, interpretation of data and formal analysis; MR and AF: planning, synthesis, aid in characterization of nanoparticles and interpretation of data. All authors read and approved the final manuscript.

Funding

Open access funding provided by The Science, Technology & Innovation Funding Authority (STDF) in cooperation with The Egyptian Knowledge Bank (EKB). This research is self-funded.

Availability of data and materials

No datasets were generated or analysed during the current study.

Declarations

Ethics approval and consent to participate

This study was waived from approval by the "Research Ethics Committee" Faculty of Dentistry, Ain Shams University, Cairo, Egypt: (FDASU-Rec ER122308).

Consent for publications

Not applicable.

Competing interests

All authors have no competing interests.

Received: 5 June 2024 Accepted: 7 January 2025

Published online: 30 January 2025

References

- Abdel-Ghany S, Mahfouz M, Ashraf N, Sabit H, Cevik E, El-Zawahri M (2020) Gold nanoparticles induce G2/M cell cycle arrest and enhance the expression of E-cadherin in breast cancer cells. *Inorg Nano-Met Chem* 50(10):926–932. <https://doi.org/10.1080/24701556.2020.1728553>
- Agarwal ML, Agarwal A, Taylor WR, Chernova O, Stark GR, Sharma Y (1998) A p53-dependent S-phase checkpoint helps to protect cells from DNA damage in response to starvation for pyrimidine nucleotides. *Proc Natl Acad Sci USA* 95(25):14775–14780. <https://doi.org/10.1073/pnas.95.25.14775>
- Alagheband Y, Jafari-gharabaghlou D, Imani M, Mousazadeh H, Dadashpour M, Firouzi-Amandi A, Zarghami N (2022) Design and fabrication of a dual-drug loaded nano-platform for synergistic anticancer and cytotoxicity effects on the expression of leptin in lung cancer treatment. *J Drug Deliv Technol* 73:103389. <https://doi.org/10.1016/j.jddst.2022.103389>
- Alexere SM, Abou-Seri HM, El-Din HES, Youssef D, Ramadan MA (2024) Green synthesis of silver and iron oxide nanoparticles mediated photothermal effects on *Blastocystis hominis*. *Lasers Med Sci* 39(1):43. <https://doi.org/10.1007/s10103-024-03984-6>
- Almessiere MA, Slimani Y, Rehman S, Khan FA, Sertkol M, Baykal A (2021) Green synthesis of Nd substituted Co-Ni nanospinel ferrites: a structural, magnetic, and antibacterial/anticancer investigation. *J Phys D Appl Phys* 55(5):055002. <https://doi.org/10.1088/1361-6463/ac2fd8/meta>
- Ansari MA, Akhtar S, Rauf MA, Alomary MN, AlYahya S, Alghamdi S, Almessiere MA, Baykal A, Khan F, Adil SF, Khan M (2021) Sol-gel synthesis of dy-substituted NiO. 4Cu0. 2Zn0. 4 (Fe2-xDyx) O4 nano spinel ferrites and evaluation of their antibacterial, antifungal, antibiofilm and anticancer potentialities for biomedical application. *Int J Nanomedicine* 18:5633–5650. <https://doi.org/10.2147/IJN.S316471>
- Bagci PO, Wang YC, Gunasekaran S (2015) A simple and green route for room-temperature synthesis of gold nanoparticles and selective colorimetric detection of cysteine. *J Food Sci* 80(9):N2071–N2078. <https://doi.org/10.1111/1750-3841.12974>

- Bandyopadhyay A, Roy B, Shaw P, Mondal P, Mondal MK, Chowdhury P, Bhattacharya S, Chattopadhyay A (2021) Chitosan-gold nanoparticles trigger apoptosis in human breast cancer cells in vitro. *The Nucleus* 64:79–92. <https://doi.org/10.1007/s13237-020-00328-x>
- Bansal SA, Kumar V, Karimi J, Singh AP, Kumar S (2020) Role of gold nanoparticles in advanced biomedical applications. *Nanoscale Adv* 2(9):3764–3787. <https://doi.org/10.1039/D0NA00472C>
- Boyles MS, Kristl T, Andosch A, Zimmermann M, Tran N, Casals E, Himly M, Puentes V, Huber CG, Lutz-Meindl U, Duschl A (2015) Chitosan functionalisation of gold nanoparticles encourages particle uptake and induces cytotoxicity and pro-inflammatory conditions in phagocytic cells, as well as enhancing particle interactions with serum components. *J Nanobiotechnol* 13:1–20. <https://doi.org/10.1186/s12951-015-0146-9>
- Bressenot A, Marchal S, Bezdetnaya L, Garrier J, Guillemin F, Plénat F (2009) Assessment of apoptosis by immunohistochemistry to active caspase-3, active caspase-7, or cleaved PARP in monolayer cells and spheroid and subcutaneous xenografts of human carcinoma. *J Histochem Cytochem* 57(4):289–300. <https://doi.org/10.1369/2Fjhc.2008.952044>
- Brown SD, Nativo P, Smith JA, Stirling D, Edwards PR, Venugopal B, Flint DJ, Plumb JA, Graham D, Wheate NJ (2010) Gold nanoparticles for the improved anticancer drug delivery of the active component of oxaliplatin. *J Am Chem Soc* 132(13):4678–4684. <https://doi.org/10.1021/ja908117a>
- Bunz F, Dutriaux A, Lengauer C, Waldman T, Zhou S, Brown JP, Sedivy JM, Kinzler KW, Vogelstein B (1998) Requirement for p53 and p21 to sustain G2 arrest after DNA damage. *Science* 282(5393):1497–1501. <https://doi.org/10.1126/science.282.5393.1497>
- Chamoli A, Gosavi AS, Shirwadkar UP, Wangdale KV, Behera SK, Kurrey NK, Kalia K, Mandoli A (2021) Overview of oral cavity squamous cell carcinoma: risk factors, mechanisms, and diagnostics. *Oral Oncol* 121:105451. <https://doi.org/10.1016/j.oraloncology.2021.105451>
- Chen J, Gao C, Zhang Y, Wang T, Qian Y, Yang B, Dong P, Zhang Y (2017) Inorganic nano-targeted drugs delivery system and its application of platinum-based anticancer drugs. *J Nanosci Nanotechnol* 17(1):1–17. <https://doi.org/10.1166/jnn.2017.12932>
- Cheng Z, Liu M, Dey R, Chen Y (2021a) Nanomaterials for cancer therapy: current progress and perspectives. *J Hematol Oncol* 14:1–27. <https://doi.org/10.1186/s13045-021-01096-0>
- Cheng Y, Li S, Gao L, Zhi K, Ren W (2021b) The molecular basis and therapeutic aspects of cisplatin resistance in oral squamous cell carcinoma. *Front Oncol* 11:761379. <https://doi.org/10.3389/fonc.2021.761379>
- Choi SY, Jeong S, Jang SH, Park J, Park JH, Ock KS, Lee SY, Joo SW (2012) In vitro toxicity of serum protein-adsorbed citrate-reduced gold nanoparticles in human lung adenocarcinoma cells. *Toxicol in Vitro* 26(2):229–237. <https://doi.org/10.1016/j.tiv.2011.11.016>
- Chompoosor A, Saha K, Ghosh PS, Macarthy DJ, Miranda OR, Zhu ZJ, Arcaro KF, Rotello VM (2010) The role of surface functionality on acute cytotoxicity, ROS generation and DNA damage by cationic gold nanoparticles. *Small* 6(20):2246–2249. <https://doi.org/10.1002/smll.201000463>
- Collado-González M, Fernández Espín V, Montalbán MG, Pamies R, Hernández Cifre JG, Díaz Baños FG, Villora G, García de la Torre J (2015) Aggregation behaviour of gold nanoparticles in presence of chitosan. *J Nanopart Res* 17:1–10. <https://doi.org/10.1007/s11051-015-3069-3>
- Dananjaya SHS, Udayangani RMC, Oh C, Nikapitiya C, Lee J, De Zoysa M (2017) Green synthesis, physio-chemical characterization and anti-candidal function of a biocompatible chitosan gold nanocomposite as a promising antifungal therapeutic agent. *RSC Adv* 7(15):9182–9193. <https://doi.org/10.1039/C6RA26915J>
- Das SK, Menezes ME, Bhatia S, Wang X, Emdad L, Sarkar D, Fisher PB (2015) Gene therapies for cancer: strategies, challenges, and successes. *J Cell Physiol* 230(2):259–271. <https://doi.org/10.1002/jcp.24791>
- Dasari S, Tchounwou PB (2014) Cisplatin in cancer therapy: molecular mechanisms of action. *Eur J Pharmacol* 740:364–378. <https://doi.org/10.1016/2Fjeiphar.2014.07.025>
- Dhar S, Daniel WL, Giljohann DA, Mirkin CA, Lippard SJ (2009) Polyvalent oligonucleotide gold nanoparticle conjugates as delivery vehicles for platinum (IV) warheads. *J Am Chem Soc* 131(41):14652–14653. <https://doi.org/10.1021/ja9071282>
- Ding J, Guo Y (2022) Recent advances in chitosan and its derivatives in cancer treatment. *Front Pharmacol* 13:888740. <https://doi.org/10.3389/fphar.2022.888740>
- Doghish AS, Hashem AH, Shehabeldine AM, Sallam AAM, El-Sayyad GS, Salem SS (2022) Nanocomposite based on gold nanoparticles and carboxymethyl cellulose: synthesis, characterization, antimicrobial, and anticancer activities. *J Drug Deliv Sci Technol* 77:103874. <https://doi.org/10.1016/j.jddst.2022.103874>
- Ellman GL (1959) Tissue sulfhydryl groups. *Arch Biochem Biophys* 82(1):70–77. [https://doi.org/10.1016/0003-9861\(59\)90090-6](https://doi.org/10.1016/0003-9861(59)90090-6)
- Faid AH, Ramadan MA (2024) Reducing the effective dose of cisplatin using cobalt modified silver nano-hybrid as a carrier on MCF7 and HCT cell models. *BMC Chem* 18(1):69. <https://doi.org/10.1186/s13065-024-01173-8>
- Faid AH, Shouman SA, Badr YA, Sharaky M (2022) Enhanced cytotoxic effect of doxorubicin conjugated gold nanoparticles on breast cancer model. *BMC Chem* 16(1):90. <https://doi.org/10.1186/s13065-022-00889-9>
- Faid AH, Hussein FEZ, Mostafa EM, Shouman SA, Badr YA, Sliem MA (2023) Hybrid chitosan gold nanoparticles for photothermal therapy and enhanced cytotoxic action of 6-mercaptopurine on breast cancer cell line. *BJBAS* 12(1):83. <https://doi.org/10.1186/s43088-023-00419-z>
- Faid AH, Rafea MA, Gad S, Sharaky M, Ramadan MA (2024) Antitumor efficiency and photostability of newly green synthesized silver/graphene oxide nanocomposite on different cancer cell lines. *Cancer Nanotechnol* 15(1):17. <https://doi.org/10.1186/s12645-024-00255-5>
- Ganji M, Dashtestani F, Neghab HK, Soheilifar MH, Hakimian F, Haghirsadat F (2021) Gold nanoparticles conjugated L-lysine for improving cisplatin delivery to human breast cancer cells. *Curr Drug Deliv* 18(6):753–760. <https://doi.org/10.2174/1567201818666201203150931>
- Gawel S, Wardas M, Niedworok E, Wardas P (2004) Malondialdehyde (MDA) as a lipid peroxidation marker. *Wiad Lek* 57(9–10):453–455
- Ghosh S (2019) Cisplatin: The first metal based anticancer drug. *Bioorg Chem* 88:102925. <https://doi.org/10.1016/j.bioorg.2019.102925>

- González-Ballesteros N, Prado-López S, Rodríguez-González JB, Lastra M, Rodríguez-Argüelles M (2017) Green synthesis of gold nanoparticles using brown algae *Cystoseira baccata*: Its activity in colon cancer cells. *Colloids Surf B Biointerfaces* 153:190–198. <https://doi.org/10.1016/j.colsurfb.2017.02.020>
- González-López MA, Gutiérrez-Cárdenas EM, Sánchez-Cruz C, Hernández-Paz JF, Pérez I, Olivares-Trejo JJ, Hernández-González O (2020) Reducing the effective dose of cisplatin using gold nanoparticles as carriers. *Cancer Nanotechnol* 11:1–15. <https://doi.org/10.1186/s12645-020-00060-w>
- Gulati S, Kumar S, Singh P, Diwan A, Mongia A (2021) Biocompatible chitosan-coated gold nanoparticles: novel, efficient, and promising nanosystems for cancer treatment. *Handbook Polymer Ceramic Nanotechnol*. https://doi.org/10.1007/978-3-030-40513-7_56
- Hamdy O, Nour M, Kamel SS, Eltayeb EA, Zaky AA, Faid AH (2024) Enhanced laser-induced fluorescence and Raman spectroscopy with gold nanoparticles for the diagnosis of oral squamous cell carcinoma. *SN Appl Sci* 6(4):157. <https://doi.org/10.1007/s42452-024-05817-1>
- Hashem AH, Shehabeldine AM, Ali OM, Salem SS (2022) Synthesis of chitosan-based gold nanoparticles: Antimicrobial and wound-healing activities. *Polymers* 14(11):2293. <https://doi.org/10.3390/polym14112293>
- Hassani N, Jafari-Gharabaghlu D, Dadashpour M, Zarghami N (2022) The effect of dual bioactive compounds artemisinin and metformin co-loaded in PLGA-PEG nanoparticles on breast cancer cell lines: potential apoptotic and anti-proliferative action. *Appl Biochem Biotechnol* 194(10):4930–4945. <https://doi.org/10.1007/s12010-022-04000-9>
- Hermeking H, Lengauer C, Polyak K, He TC, Zhang L, Thiagalingam S, Kinzler KW, Vogelstein B (1997) 14–3–3 σ is a p53-regulated inhibitor of G2/M progression. *Mol Cell* 1(1):3–11. [https://doi.org/10.1016/s1097-2765\(00\)80002-7](https://doi.org/10.1016/s1097-2765(00)80002-7)
- Ho GY, Woodward N, Coward JIG (2016) Cisplatin versus carboplatin: comparative review of therapeutic management in solid malignancies. *Crit Rev Oncol Hemat* 102:37–46. <https://doi.org/10.1016/j.critrevonc.2016.03.014>
- Jafari-Gharabaghlu D, Dadashpour M, Khanghah OJ, Salmani-Javan E, Zarghami N (2023) Potentiation of Folate-Functionalized PLGA-PEG nanoparticles loaded with metformin for the treatment of breast Cancer: possible clinical application. *Mol Biol Rep* 50(4):3023–3033. <https://doi.org/10.1007/s11033-022-08171-w>
- Javed MN, Dahiya ES, Ibrahim AM, Alam MS, Khan FA, Pottoo FH (2020) recent advancement in clinical application of nanotechnological approached targeted delivery of herbal drugs. In: Beg S, Barkat M, Ahmad F (eds) *Nanophytomedicine*. Springer, Singapore. https://doi.org/10.1007/978-981-15-4909-0_9
- Jayasuriya AC, Darr A J (2013) Controlled release of cisplatin and cancer cell apoptosis with cisplatin encapsulated poly (lactic-co-glycolic acid) nanoparticles. <https://doi.org/10.4236/jbise.2013.65074>
- Kannappan R, Ravindran J, Prasad S, Sung B, Yadav VR, Reuter S, Chaturvedi MM, Aggarwal BB (2010) γ -Tocotrienol promotes TRAIL-induced apoptosis through reactive oxygen species/extracellular signal-regulated kinase/p53-mediated upregulation of death receptors. *Mol Cancer Ther* 9(8):2196–2207. <https://doi.org/10.1158/1535-7163.MCT-10-0277>
- Kanwal Z, Raza MA, Riaz S, Manzoor S, Tayyeb A, Sajid I, Naseem S (2019) Synthesis and characterization of silver nanoparticle-decorated cobalt nanocomposites (Co@ AgNPs) and their density-dependent antibacterial activity. *R Soc Open Sci* 6(5):182135. <https://doi.org/10.1098/rsos.182135>
- Kenchegowda M, Rahamathulla M, Hani U, Begum MY, Guruswamy S, Osmani RA, Gowrav MP, Alshehri S, Ghoneim MM, Alshlowi A, Gowda DV (2021) Smart nanocarriers as an emerging platform for cancer therapy: a review. *Molecules* 27(1):146. <https://doi.org/10.3390/molecules27010146>
- Khamaikawin W, Locharoenrat K (2023) Evaluation of a docetaxel-cisplatin-fluorouracil-Au complex in human oral carcinoma cell line. *Artif Cells Nanomed Biotechnol* 51(1):148–157. <https://doi.org/10.1080/21691401.2023.2189913>
- Khan FA, Akhtar S, Almohazey D, Alomari M, Almofty SA, Eliassari A (2018) Fluorescent magnetic submicronic polymer (FMSP) nanoparticles induce cell death in human colorectal carcinoma cells. *Artif Cells Nanomed Biotechnol* 46(3):247–253. <https://doi.org/10.1080/21691401.2018.1491476>
- Khan FA, Lammari N, Muhammad Siar AS, Alkhater KM, Asiri S, Akhtar S, Almansour I, Alamoudi W, Haroun W, Louaer W, Meniai AH (2020) Quantum dots encapsulated with curcumin inhibit the growth of colon cancer, breast cancer and bacterial cells. *Nanomedicine* 15(10):969–980. <https://doi.org/10.2217/nnm-2019-0429>
- Khoshravan Azar L, Dadashpour M, Hashemi M, Zarghami N (2022) Design and development of nanostructured co delivery of artemisinin and chrysin for targeting hTERT gene expression in breast cancer cell line: possible clinical application in cancer treatment. *Apjcp* 23(3):919. <https://doi.org/10.31557/apjcp.2022.23.3.919>
- Kielkopf CL, Bauer W (2020) Urbatsch IL (2020) bradford assay for determining protein concentration. *Cold Spring Harb Protoc* 4:102269. <https://doi.org/10.1101/pdb.prot102269>
- Krogerus LA, Andersson LC (1988) A simple method for the preparation of paraffin-embedded cell blocks from fine needle aspirates, effusions and brushings. *Acta Cytol* 32:585–587
- Kubo T, Morikawa M, Ohba H, Fujii M (2003) Synthesis of DNA-peptide conjugates by solid-phase fragment condensation. *Org Lett* 5(15):2623–2626. <https://doi.org/10.1021/ol034721p>
- Li Z, Liu Y, Wang F, Gao Z, Elhefny MA, Habotta OA, Abdel Moniem AE, Kassab RB (2021) Neuroprotective effects of protocatechuic acid on sodium arsenate induced toxicity in mice: Role of oxidative stress, inflammation, and apoptosis. *Chem Biol Interact* 337:109392. <https://doi.org/10.1016/j.cbi.2021.109392>
- Li J, Fu J, Tian X, Hua T, Poon T, Koo M, Chan W (2022) Characteristics of chitosan fiber and their effects towards improvement of antibacterial activity. *Carbohydr Polym* 280:119031. <https://doi.org/10.1016/j.carbpol.2021.119031>
- Liu M, Gu X, Zhang K, Ding Y, Wei X, Zhang X, Zhao Y (2013) Gold nanoparticles trigger apoptosis and necrosis in lung cancer cells with low intracellular glutathione. *J Nanoparticle Res* 15:1–14. <https://doi.org/10.1007/s11051-013-1745-8>
- Lorenzo-Anota HY, Zarate-Triviño DG, Uribe-Echeverría JA, Ávila-Ávila A, Rangel-López JR, Martínez-Torres AC, Rodríguez-Padilla C (2021) Chitosan-coated gold nanoparticles induce low cytotoxicity and low ROS production in primary leucocytes, independent of their proliferative status. *Pharmaceutics* 13(7):942. <https://doi.org/10.3390/pharmaceutics13070942>

- Luk SCW, Siu SWF, Lai CK, Wu YJ, Pang SF (2005) Cell cycle arrest by a natural product via G2/M checkpoint. *Int J Med Sci* 2(2):64–69. <https://doi.org/10.7150/ijms.2.64>
- Ma P, Xiao H, Li C, Dai Y, Cheng Z, Hou Z, Lin J (2015) Inorganic nanocarriers for platinum drug delivery. *Mater Today* 18(10):554–564. <https://doi.org/10.1016/j.mattod.2015.05.017>
- Martínez-Torres AC, Zarate-Triviño DG, Lorenzo-Anota HY, Ávila-Ávila A, Rodríguez-Abrego C, Rodríguez-Padilla C (2018) Chitosan gold nanoparticles induce cell death in HeLa and MCF-7 cells through reactive oxygen species production. *Int J Nanomed* 13:3235–3250. <https://doi.org/10.2147/2FJN.S165289>
- Martínez-Torres AC, Lorenzo-Anota HY, García-Juárez MG, Zarate-Triviño DG, Rodríguez-Padilla C (2019) Chitosan gold nanoparticles induce different ROS-dependent cell death modalities in leukemic cells. *Int J Nanomed* 14:7173–7190. <https://doi.org/10.2147/2FJN.S221021>
- Miranda KM, Espey MG, Wink DA (2001) A rapid, simple spectrophotometric method for simultaneous detection of nitrate and nitrite. *Nitric Oxide* 5(1):62–71. <https://doi.org/10.1006/niox.2000.0319>
- Mohamad EA, Rageh M, Ezz-Aldoula RA, Ramadan MA (2023) Examination of the interaction between bovine albumin and gold nanoparticles. *Egypt J Chem* 66(13):1689–1694. <https://doi.org/10.21608/ejchem.2023.223345.8267>
- Mohanpuria P, Rana NK, Yadav SK (2008) Biosynthesis of nanoparticles: technological concepts and future applications. *J Nanoparticle Res* 10:507–517. <https://doi.org/10.1007/s11051-007-9275-x>
- Mullen P (2004) Flow cytometric DNA analysis of human cancer cell lines. In: Langdon, S.P. (eds) *cancer cell culture. Methods in Molecular Medicine™*. Humana Press, 88, 247–255. <https://doi.org/10.1385/1-59259-406-9:247>
- Nejati K, Dadashpour M, Gharibi T, Mellatyar H, Akbarzadeh A (2022) Biomedical applications of functionalized gold nanoparticles: a review. *J Clust Sci* 33:1–6. <https://doi.org/10.1007/s10876-020-01955-9>
- Oun R, Moussab YE, Wheate NJ (2018) The side effects of platinum based chemotherapy drugs: a review for chemists. *Dalton Trans* 47(19):6645–6653. <https://doi.org/10.1039/c8dt00838h>
- Park EJ, Choi KS, Yoo YH, Kwon TK (2013) Nutlin-3, a small-molecule MDM2 inhibitor, sensitizes Caki cells to TRAIL-induced apoptosis through p53-mediated PUMA upregulation and ROS-mediated DR5 upregulation. *Anticancer Drugs* 24(3):260–269. <https://doi.org/10.1097/cad.0b013e32835c0311>
- Pourgholi A, Dadashpour M, Mousapour A, Amandi AF, Zarghami N (2021) Anticancer potential of silibinin loaded polymeric nanoparticles against breast cancer cells: insight into the apoptotic genes targets. *Apjcp* 22(8):2587. <https://doi.org/10.31557/2FAPJCP.2021.22.8.2587>
- Pucelik B, Sufek A, Borkowski M, Barzowska A, Kobielusz M, Dąbrowski JM (2022) Synthesis and characterization of size- and charge-tunable silver nanoparticles for selective anticancer and antibacterial treatment. *ACS Appl Mater Interfaces* 14(13):14981–14996. <https://doi.org/10.1021/acsmi.2c01100>
- Ramadan MA, El-Tayeb TA (2023) Photostability, cytotoxicity, and photothermal impact of AgNPs, CoAgNC, and IOAgNC on Hep-2 laryngeal carcinoma cells. *SN Appl Sci* 5:253. <https://doi.org/10.1007/s42452-023-05472-y>
- Ramadan MA, Sharaky M, Faid AH (2022) Ionic gelation synthesis, characterization and cytotoxic evaluation of chitosan nanoparticles on different types of human cancer cell models. *Egypt J Chem* 65(2):153–159. <https://doi.org/10.21608/ejchem.2021.82733.4070>
- Ramadan MA, Sharaky M, Gad S, Ahmed HA, Jaremko M, Emwas AH, Faid AH (2024a) A Anticancer effect and laser photostability of ternary graphene oxide/chitosan/silver nanocomposites on various cancer cell lines. *Nanomed* 19(8):709–722. <https://doi.org/10.2217/nnm-2023-0264>
- Ramadan MA, Gad S, Sharaky M, Faid AH (2024b) Laser photostability of chitosan coated gold-GO nanocomposite and its role as a nano-therapeutic agent for control breast cancer growth. *SN App Sci* 6(4):1–12. <https://doi.org/10.1007/s42452-024-05808-2>
- Reen DJ (1994) Enzyme-linked immunosorbent assay (ELISA). In: Walker, J.M. (eds) *Basic protein and peptide protocols. Methods in Molecular Biology™*, vol 32. Humana Press: 461–466. <https://doi.org/10.1385/0-89603-268-x:461>
- Regiel-Futyr A, Kus-Liškiewicz M, Sebastian V, Irueta S, Arruebo M, Stochel G, Kyzioł A (2015) Development of noncytotoxic chitosan-gold nanocomposites as efficient antibacterial materials. *ACS Appl Mater Interfaces* 7(2):1087–1099. <https://doi.org/10.1021/am508094e>
- Rocha CRR, Silva MM, Quinet A, Cabral-Neto JB, Menck CFM (2018) DNA repair pathways and cisplatin resistance: an intimate relationship. *Clinics* 73(1):e478s. <https://doi.org/10.6061/2Fclinics/2F2018/2Fe478s>
- Saha S, Xiong X, Chakraborty PK, Shameer K, Arvizo RR, Kudgus RA, Dwivedi SK, Hossen MN, Gillies EM, Robertson JD, Dudley JT (2016) Gold nanoparticle reprograms pancreatic tumor microenvironment and inhibits tumor growth. *ACS Nano* 10(12):10636–10651. <https://doi.org/10.1021/acsnano.6b02231>
- Salah A, Hassab-Elnaby S, Ramadan MA (2023) Boosting the nonlinear optical absorption of graphene oxide, and gold nanorods by tailoring graphene oxide-gold nanorods hybrids. *SN Appl Sci* 5(11):288. <https://doi.org/10.1007/s42452-023-05507-4>
- Sancho-Martínez SM, Prieto-García L, Prieto M, Lopez-Novoa JM, López-Hernández FJ (2012) Subcellular targets of cisplatin cytotoxicity: an integrated view. *Pharmacol Therapeut* 136(1):35–55. <https://doi.org/10.1016/j.pharmthera.2012.07.003>
- Saravanakumar K, Mariadoss AVA, Sathiyaseelan A, Wang MH (2020) Synthesis and characterization of nano-chitosan capped gold nanoparticles with multifunctional bioactive properties. *Int J Biol Macromol* 165(Pt A):747–757. <https://doi.org/10.1016/j.jbiomac.2020.09.177>
- Selim ME, Hendi AA (2012) Gold nanoparticles induce apoptosis in MCF-7 human breast cancer cells. *APJCP* 13(4):1617–1620. <https://doi.org/10.7314/APJCP.2012.13.4.1617>
- Shaaban A, Salem A, Elramly F, Ahmed E, Moawed F, Hegazy MGE (2022) Newly created hybrid nanomaterial for treatment of lung carcinoma. *Egypt J Chem* 65(131):1543–1550. <https://doi.org/10.21608/ejchem.2022.134874.6127>
- Sharaky M, Kamel M, Aziz MA, Omran M, Rageh MM, Abouzid KA, Shouman SA (2020) Design, synthesis and biological evaluation of a new thieno [2, 3-d] pyrimidine-based urea derivative with potential antitumor activity against tamoxifen sensitive and resistant breast cancer cell lines. *J Enzyme Inhib Med Chem* 35(1):1641–1656. <https://doi.org/10.1080/2F14756366.2020.1804383>

- Skowron M, Melnikova M, van Roermund J, Romano A, Albers P, Thomale J, Schulz WA, Niegisch G, Hoffmann M (2018) Multifaceted mechanisms of cisplatin resistance in long-term treated urothelial carcinoma cell lines. *Int J Mol Sci* 19(2):590. <https://doi.org/10.3390/ijms19020590>
- Takimoto H, Hasegawa M, Yagi K, Nakamura T, Sakaeda T, Hirai M (2004) Proapoptotic effect of a dietary supplement: water soluble chitosan activates caspase-8 and modulating death receptor expression. *DMPK* 19(1):76–82. <https://doi.org/10.2133/dmpk.19.76>
- Troy D, Baudino A (2015) Targeted cancer therapy: the next generation of cancer treatment. *Curr Drug Discov Technol* 12(1):3–20. <https://doi.org/10.2174/1570163812666150602144310>
- Tsikis D (2017) Assessment of lipid peroxidation by measuring malondialdehyde (MDA) and relatives in biological samples: analytical and biological challenges. *Anal Biochem* 524:13–30. <https://doi.org/10.1016/j.ab.2016.10.021>
- Vichai V, Kirtikara K (2006) Sulforhodamine B colorimetric assay for cytotoxicity screening. *Nat Protoc* 1(3):1112–1116. <https://doi.org/10.1038/nprot.2006.179>
- Wimardhani YS, Suniarti DF, Freisleben HJ, Wanandi SI, Siregar NC, Ikeda MA (2014) Chitosan exerts anticancer activity through induction of apoptosis and cell cycle arrest in oral cancer cells. *J Oral Sci* 56(2):119–126. <https://doi.org/10.2334/josnurd.56.119>
- Wiranowska M, Singh R, Falahat R, Williams E, Johnson JO, Alcantar N (2020) Preferential drug delivery to tumor cells than normal cells using a tunable niosome–chitosan double package nanodelivery system: a novel in vitro model. *Cancer Nanotechnol* 11:1–20. <https://doi.org/10.1186/s12645-020-00059-3>
- Wróblewska AM, Milewska A, Drozd MM (2022) Targeted delivery of cisplatin by gold nanoparticles: the influence of nanocarrier surface modification type on the efficiency of drug binding examined by CE-ICP-MS/MS. *Int J Mol Sci* 23(4):2324. <https://doi.org/10.3390/ijms23042324>
- Zenjanab MK, Pakchin PS, Fathi M, Abdolahinia ED, Adibkia K (2024) Niosomes containing paclitaxel and gold nanoparticles with different coating agents for efficient chemo/photothermal therapy of breast cancer. *Biomed Mater* 19(3):035015. <https://doi.org/10.1088/1748-605x/ad2ed5>
- Zhang H, Chen J (2018) Current status and future directions of cancer immunotherapy. *J Cancer* 9(10):1773–1781. <https://doi.org/10.7150/jca.24577>
- Zhang L, Zhai BZ, Wu YJ, Wang Y (2023) Recent progress in the development of nanomaterials targeting multiple cancer metabolic pathways: a review of mechanistic approaches for cancer treatment. *Drug Delivery* 30(1):1–18. <https://doi.org/10.1080/10717544.2022.2144541>

Publisher's Note

Springer Nature remains neutral with regard to jurisdictional claims in published maps and institutional affiliations.